# Inhibition of G-protein-coupled receptor kinase 2 prevents the dysfunctional cardiac substrate metabolism in fatty acid synthase-transgenic mice

Abd Alla, Joshua ; Graemer, Muriel ; Fu, Xuebin ; Quitterer, Ursula

Abstract: Impairment of myocardial fatty acid substrate metabolism is characteristic of late-stage heart failure and has limited treatment options. Here we investigated whether inhibition of G-protein-coupled receptor kinase 2 (GRK2) could counteract the disturbed substrate metabolism of late-stage heart failure. The heart failure-like substrate metabolism was reproduced in a novel transgenic model of myocardium-specific expression of fatty acid synthase (FASN), the major palmitate-synthesizing enzyme. The increased fatty acid utilization of FASN-transgenic neonatal cardiomyocytes rapidly switched to a heart failure phenotype in an adult-like lipogenic milieu. Similarly, adult FASN-transgenic mice developed signs of heart failure. The development of disturbed substrate utilization of FASN-transgenic cardiomyocytes and signs of heart failure were retarded by the transgenic expression of GRKInh, a peptide inhibitor of GRK2. Cardioprotective GRK2 inhibition required an intact ERK (extracellular signal-regulated kinase) axis, which blunted the induction of cardiotoxic transcripts, in part by enhanced serine-273 phosphorylation of Pparg (peroxisome proliferator-activated receptor ). Conversely, the dual-specific GRK2 and ERK cascade inhibitor, RKIP (raf kinase inhibitor protein), triggered dysfunctional cardiomyocyte energetics and the expression of heart failure-promoting Pparg-regulated genes. Thus, GRK2 inhibition is a novel approach that targets the dysfunctional substrate metabolism of the failing heart.

DOI: https://doi.org/10.1074/jbc.M115.702688

JBC Papers in Press. Published on December 15, 2015 as Manuscript M115.702688
The latest version is at http://www.jbc.org/cgi/doi/10.1074/jbc.M115.702688


# Inhibition of G-Protein-Coupled Receptor Kinase 2 Prevents the Dysfunctional Cardiac Substrate Metabolism in Fatty Acid Synthase-Transgenic Mice

**Joshua Abd Alla[1], Muriel Graemer[1], Xuebin Fu[1,2], and Ursula Quitterer[1,3]**

[1]From the Department of Chemistry and Applied Biosciences, Molecular Pharmacology Unit, Swiss Federal Institute of Technology (ETH) Zurich, 8057 Zurich, Switzerland
[2]Department of Clinical Research, University of Bern, 3010 Bern, Switzerland
[3]Department of Medicine, Institute of Pharmacology and Toxicology, University of Zurich, 8057 Zurich, Switzerland

Running title: GRK2 inhibition retards cardiometabolic dysfunction

To whom correspondence should be addressed: Prof. Ursula Quitterer, Molecular Pharmacology Unit, ETH Zurich, Winterthurerstrasse 190, CH-8057 Zurich, Switzerland, Telephone: +41 44 6356001; FAX: +41 44 6356881; E-mail: ursula.quitterer@pharma.ethz.ch

**Keywords:** Cardiac metabolism, extracellular signal-regulated kinase (ERK), fatty acid synthase, G-protein-coupled receptor kinase 2 (GRK2; ADRBK1), heart failure, microarray, peroxisome proliferator-activated receptor (PPAR), transgenic mice

## ABSTRACT

Impairment of myocardial fatty acid substrate metabolism is characteristic of late-stage heart failure and has limited treatment options. Here we investigated whether inhibition of G-protein-coupled receptor kinase 2 (GRK2) could counteract the disturbed substrate metabolism of late-stage heart failure. The heart failure-like substrate metabolism was reproduced in a novel transgenic model of myocardium-specific expression of fatty acid synthase (FASN), the major palmitate-synthesizing enzyme. The increased fatty acid utilization of *FASN*-transgenic neonatal cardiomyocytes rapidly switched to a heart failure phenotype in an adult-like lipogenic milieu. Similarly, adult *FASN*-transgenic mice developed signs of heart failure. The development of disturbed substrate utilization of *FASN*-transgenic cardiomyocytes and signs of heart failure were retarded by the transgenic expression of GRKInh, a peptide inhibitor of GRK2. Cardioprotective GRK2 inhibition required an intact ERK (extracellular signal-regulated kinase) axis, which blunted the induction of cardiotoxic transcripts, in part by enhanced serine-273 phosphorylation of *Pparg* (peroxisome proliferator-activated receptor γ). Conversely, the dual-specific GRK2 and ERK cascade inhibitor, RKIP (raf kinase inhibitor protein), triggered dysfunctional cardiomyocyte energetics and the expression of heart failure-promoting *Pparg*-regulated genes. Thus, GRK2 inhibition is a novel approach that targets the dysfunctional substrate metabolism of the failing heart.

Heart failure is a debilitating syndrome that involves insufficient cardiac performance. Multiple pathomechanisms have been elucidated but treatment options remain insufficient, and hence the mortality of heart failure is high (1). The causes of heart failure are complex with ischemic heart disease being the most frequently associated condition (2). Co-existing disorders such as diabetes, hypertension and obesity, further deteriorate symptoms (3). Despite having a different aetiology, late-stage heart failure is commonly characterised by severe changes in myocardial substrate metabolism, with a switch from fatty acid oxidation towards predominant glycolysis (4-6). Conflicting evidence exists as to whether this substrate switch is beneficial or detrimental (7), but several previous studies have indicated that an increased availability of lipid substrates that counteract the substrate switch could improve cardiac function (7,8). Moreover, treatment options, which improve substrate availability, are attractive because the failing heart is often considered to be "an engine, running out of fuel" (9).

Following this concept, we aimed to investigate the impact of improved cardiac substrate availability by generating transgenic

mice with myocardium-specific expression of fatty acid synthase (*FASN*), the major palmitate-synthesizing enzyme. Such an approach is also supported by data obtained for myocardium-specific *Fasn* deficiency, which have revealed the cardioprotective potential of *Fasn* (10). On the other hand, hearts from patients with heart failure showed an increased expression and protein level of FASN (10,11). By generation of transgenic mice, we found that *FASN*-transgenic mice developed a heart failure-like phenotype with impaired cardiomyocyte substrate use. In search for a treatment approach for the disturbed cardiac substrate metabolism, we focused on the role of GRK2 inhibition because GRK2 inhibition could counteract cardiolipotoxicity by promotion of a cardiomyocyte survival program (12,13), and resensitization of the cardioprotective adiponectin receptor 1 (14-16). For GRK2 inhibition in vivo, we used GRKInh, a small peptide inhibitor derived from the first intracellular loop of the β2-adrenergic receptor (12,17). Our data with GRKInh show that GRK2 inhibition counteracts the heart failure-related cardiac metabolic dysfunction and signs of heart failure of *FASN*-transgenic mice.

## EXPERIMENTAL PROCEDURES

*Generation of transgenic mice and animal experiments*–Transgenic mice were generated as described (12) with minor modifications. Briefly, for the generation of transgenic mice with myocardium-specific expression of *FASN*, we constructed a transgenc that placed the *FASN* cDNA under the control of the α-MHC (α-myosin heavy chain) promoter (12). For the generation of transgenic mice with myocardium-specific expression of *UCP1* (uncoupling protein-1), *PPARG* and *PPARG-S273A* (isoform-1, which lacks amino acids 1-28 of isoform-2; serine-273 refers to the numbering of isoform-2) a similar approach was used. The plasmid sequence was removed by NotI digestion, and the purified linear DNA (2 ng/ml) was injected into fertilised oocytes of superovulated B6 (C57BL/6J) mice. For generation of transgenic Tg-*PPARG* and Tg-*PPARG-S273A* mice, fertilized oocytes from non-transgenic and Tg-GRKInh mice (transgenic mice with myocardium-specific expression of GRKInh, a GRK2-specific peptide inhibitor with the peptide sequence MAKFERLQTVTNYFITSE) were used. Transgenic mice with myocardium-specific expression of GRKInh or human RKIP (*PEBP1*) were generated and characterized previously (12). Mouse lines in the study were deposited into the JAX repository (The Jackson Laboratory, USA) and have the following strain ID numbers: 911818 [C57BL/6Tg(MHCPEBP1)1 Sjaa]; 911822 [C57BL/6Tg(MHCGRK-Inh)1 Sjaa]; 911826 [C57BL/6Tg(MHCFASN)1 Sjaa]; 911830 [C57BL/6Tg(MHCUCP1)1 Sjaa].

The effect of rosiglitazone-induced *Pparg* activation was analysed with 8 month-old male ApoE-/- mice, which had received 30 mg/kg/d rosiglitazone for two months. Untreated, age-matched ApoE-/-, and non-transgenic B6 mice served as control groups. Abdominal aortic constriction (AAC) was performed in 4 month-old male B6 mice to trigger pressure overload-induced cardiac hypertrophy and signs of heart failure (11). Age-matched control mice underwent the identical surgical procedure except for ligation of the aorta (sham-operated mice). All of the mice were kept on a 12 h light/12 h dark regime, and had free access to food and water. The ApoE-/- mice were fed a rodent chow that contained 7 % fat and 0.15 % cholesterol (AIN-93-based diet) whereas B6 mice were fed a standard rodent chow containing 4.5 % fat.

Transthoracic echocardiography was performed with a Vivid 7 echocardiograph equipment (GE Healthcare) with a 12 MHz linear array transducer similarly as previously described (11). The left ventricular ejection fraction was calculated in the M-mode of the parasternal long-axis view using the formula of Teichholz. Recordings were interpreted offline using EchoPac Pc 3.0 software (GE).

Animal experiments were performed in accordance with the NIH guidelines, and reviewed and approved by the local committee on animal care and use (University of Zurich).

*Whole genome microarray gene expression analysis*–Whole genome microarray gene expression analysis of cardiac tissue was performed using Affymetrix GeneChip Mouse genome MG430 2.0 Arrays essentially as described previously (18). GO (gene ontology) analyses of microarray data were performed with GCOS and/or RMA-processed data using GeneSpring GX software (Agilent). Probe sets, which were significantly up-regulated in failing hearts (fold change ≥ 2 relative to the respective control group and $P \leq 0.01$) were used for GO

classification. Microarray gene expression data are available at the NCBI GEO database accession numbers GSE25765-8 (GSE25765, GSE25766, GSE25767, GSE25768), GSE28031 and GSE49351.

Gene expression of selected genes was also analysed by real-time quantitative (q) RT-PCR with a LightCycler 480 (Roche Diagnostics). Sequences of the forward and reverse primers were as follows: *Acaca* forward 5`-GCCTCCGTCAGCTCAGATAC-3`; *Acaca* reverse 5`-GACCACCGACGGATAGATCG-3`; *Adipoq* forward 5`-ACTGCAACATTCCGGGACTC-3`; *Adipoq* reverse 5`-GAGGCCTGGTCCACATTCTT-3`; *Fasn* forward 5`-GGCCCCTCTGTTAATTGGCT-3`; *Fasn* reverse 5`-CGCTTGTTGGTGGACACTTG-3`; *FASN* forward 5`-TCGTGTTGACTTCTCGCTCC-3`; *FASN* reverse 5`-AAGCCGTAGTTGCTCTGTCC-3`; *PPARG* forward 5`-GCTCCGTGGATCTCTCCGTA-3`; *PPARG* reverse 5`-AGCTTTATCTCCACAGACACGA-3`; *Retn* forward 5`-GTCCTGCTAAGTCCTCTGCCAC-3`; *Retn* reverse 5`-GGCTGCTGTCCAGTCTATCCTTG-3`; *Ucp1* forward 5`-CACTGCCAAAGTCCGCCTTCAGA-3`; and *Ucp1* reverse 5`-GCAGGCAGACCGCTGTACAGTT-3`.

*Lentiviral-mediated down regulation of Fasn and Ucp1 by RNAi in vivo*–For the down regulation of *Fasn* expression in vivo, ApoE$^{-/-}$ mice were transduced by i.p. administration of a replication-incompetent lentivirus ($1x10^8$ copies/mouse in PBS), which down-regulates *Fasn* by polymerase II (Pol II)-dependent expression of a pre-miRNA targeting the *Fasn* RNA by RNAi. Endogenously expressed *Ucp1* was down-regulated by the transduction of B6 mice with a lentivirus that expressed a pre-miRNA targeting *Ucp1* by RNAi. The lentiviral expression plasmids were generated by inserting the indicated double-stranded oligonucleotides that encoded an engineered pre-miRNA sequence into the pLenti6/V5-Dest Gateway® Vector (Invitrogen): mi*Fasn* top strand 5'-TGCTGATAACTTGGAGTTCGGGTCTTGTTT TGGCCACTGACTGACAAGACCCGCTCCAA GTTAT-3`; mi*Fasn* bottom strand 5'-CCTGATAACTTGGAGCGGGTCTTGTCAGTC AGTGGCCAAAACAAGACCCGAACTCCAAG TTATC-3'; mi*Ucp1* top strand 5`-TGCTGTTTGATCCCATGCAGATGGCTGTTT TGGCCACTGACTGACAGCCATCTATGGGAT CAAA-3; and mi*Ucp1* bottom strand 5`-CCTGTTTGATCCCATAGATGGCTGTCAGTC AGTGGCCAAAACAGCCATCTGCATGGGAT CAAAC-3. A pseudotyped lentivirus was produced by cotransfection of 293FT cells with the lentiviral plasmid and a mixture of packaging plasmids pLP1, pLP2 and pLP/VSVG (Invitrogen). To quantify the lentivirus integration in vivo, we used primers that comprised sequences that were derived from the cytomegalovirus immediate early promoter and the pre-miRNA-sequence. Down regulation of *Fasn* (or *Ucp1*) expression was confirmed by real-time qRT-PCR after the transduction of mice or isolated neonatal mouse cardiomyocytes with mi*Fasn*-lentivirus (or mi*Ucp1*-lentivirus).

*Antibodies*–The following antibodies were used for immunohistochemistry, immunofluorescence and immunoblotting: anti-ARRB1 (beta-arrestin-1) antibodies, raised in mouse against recombinant ARRB1 (12); anti-Agtr1 (AT1R) antibodies, which were raised in rat against the carboxyl-terminal region of Agtr1 (19); anti-FASN antibodies, which were raised in rabbit against an antigen encompassing amino acids 2205-2504 of FASN (11); anti-GRK2 (ADRBK1) antibodies, raised in rabbit against recombinant GRK2 protein (12); anti-GRK5 antibodies, raised in rabbit against recombinant GRK5 protein (12); anti-GRKInh antibodies, raised in rabbit against GRKInh (12); anti-Pparg antibodies, raised in rabbit against an antigen encompassing amino acids 8-106 of Pparg (Santa Cruz Biotechnology Inc., USA) or synthetic phosphopeptides derived from PPARG around the phosphorylation site of S273 or S112 (BIOSS antibodies; Abcam); and Ucp1/UCP1 antibodies were raised in rabbit against an antigen encompassing amino acids 288-302 of mouse/human Ucp1/UCP1 (11). For the immunohistological and immunoblot detection of activated phospho-ERK1/2, phospho-ERK1/2-specific antibodies were used detecting activated ERK1/2 phosphorylated at T202+Y204 of ERK1, and T185+Y187 of ERK2 (E10 mouse mAb, Cell Signaling). For immunoblot detection of ERK1/2 ERK1/2-specific antibodies raised in rabbit (Cell Signaling) were used, and immunofluorescence detection of p38 MAPK (mitogen-activated

protein kinase) on cardiac sections was performed with anti-p38 antibodies (Cell Signalling). The immunoblot detection of activated AMPKα (Prkaa1/2; protein kinase, AMP-activated alpha 1/2 catalytic subunit) phosphorylated on T183/172 was detected with antibodies raised in rabbit against a synthetic peptide corresponding to residues that surrounded T172 (40H9, Cell Signaling). Immunoblotting and immunohistochemistry were routinely used to determine and confirm the cross-reactivity of the antibodies with the respective mouse and human proteins.

*Immunohistology analyses and immunofluorescence*–For immunohistology, we used paraffin sections or cryosections of mouse heart specimens. Immunohistological detection of Fasn (FASN) was performed with affinity-purified, polyclonal antibodies as described (11). Methods describing oil red O staining, immunofluorescence detection of proteins, and immunohistology for activated phospho-ERK1/2 in paraffin sections or cryosections have been described previously (11,12). Immunohistology sections were imaged with a Leica DMI6000 microscope equipped with a DFC420 camera, and immunofluorescence imaging was performed with a Leica (TCS) confocal laser microscope.

*Immunoblot detection of proteins*–For immunoblot detection of proteins, cardiac tissue was pulverized in liquid nitrogen and extracted with RIPA buffer supplemented with protease/phosphatase inhibitor cocktail, as previously described (20). Detection of proteins was performed with affinity-purified antibodies or $F(ab)_2$ fragments of the respective antibodies (11,12) after separation of proteins by SDS-PAGE and subsequent electrophoretic protein transfer to PVDF membranes. Bound antibody was visualised with $F(ab)_2$ fragments of enzyme-coupled secondary antibodies (Dianova), or by enzyme-coupled protein A (Merck Millipore) as applicable, and was followed by enhanced chemiluminescent detection (ECL Prime, Amersham).

*Functional assays*–Mouse or rat neonatal cardiomyocytes were isolated and transfected as described (12,21). Fibroblasts were removed by preplating for 1 h at 37°C. Cardiomyocytes were collected and cultivated in MEM [minimum essential medium supplemented with 5 % FCS and 25 mg/l BrdU (5-bromo-2`-deoxyuridine)]. For knockdown of *Fasn* and *Ucp1*, neonatal cardiomyocytes were transfected with stealth RNAi targeting the coding sequence of rat or mouse *Fasn* (nucleotides 428-452 and 1990-2014; Invitrogen) and *Ucp1* (nucleotides 289-313 and 401-425; Invitrogen). For cardiomyocyte expression of *PPARG* and *PPARG-S273A*, the human cDNAs encoding *PPARG* and *PPARG-S273A*, were inserted into the KpnI/XbaI sites of pcDNA3 (Invitrogen). All of the mutants and constructs that were generated by PCR were sequenced entirely. DNA strand breaks were determined in situ by the terminal deoxynucleotidyl transferase-mediated dUTP nick-end labeling (TUNEL) technique (Roche Applied Science) (12). Measurement of the [ATP] of cardiac tissue extracts was performed as described (11), and *Pparg* transcription factor DNA binding activity was determined with a *Pparg* transcription factor assay kit (Abcam). Cellular cAMP, total cardiac free fatty acids (FFA) and triacylglycerol (TAG) contents were analysed as detailed previously (11,21). Cardiac contents of diacylglycerol (DAG) and ceramides were determined with the DAG kinase assay method as described (22).

*Measurement of cardiomyocyte substrate metabolism*–We used a Seahorse XF24 Extracellular Flux Analyzer (Seahorse Bioscience) to determine the cardiomyocyte substrate metabolism. The oxygen consumption rates, OCR (pmol/min), and extracellular acidification rates, ECAR (the $H^+$ production rate, mpH/min), of neonatal cardiomyocytes (10 000 cells/well) plated on Cell-Tak-coated plates (Discovery Labware Inc., Bedford, MA, USA) were measured in assay medium (i.e., unbuffered DMEM supplemented with 5.5 mM glucose and 0.5 mM carnitine) according to the Installation and Operation Manual from Seahorse Bioscience. The oxidation of endogenous fatty acids (without exogenously added palmitate, to detect the function of transgenic *FASN* expression) was determined by measurement of the absolute and relative OCR that was inhibited by the CPT-1 (carnitine palmitoyl transferase 1) inhibitor, Etomoxir (50 μM). The extent of glycolysis was determined by measurement of the absolute and relative ECAR, which was inhibited by 50 mM 2-deoxyglucose (2-DG). As indicated, we also determined the effect of an adult-like lipogenic milieu by the cultivation of cardiomyocytes for 10 days with a

3F protocol that consisted of insulin (5 μg/ml), 3-isobutylmethylxanthine (IBMX; 0.25 mM) and dexamethasone (0.5 μM) (23), which were added as supplements to the standard medium. As a control for the 3F protocol, we used cardiomyocytes that were cultivated for 10 days under standard conditions. Long-term cultivation of neonatal cardiomyocytes is a model of in vitro senescence characterized by metabolic deficiencies (24), which could account for the overall low β-oxidation rate of 5-25 % in our experiments. Metabolic flux experiments were performed on 6 wells of a 24-well plate (technical replicates), and were reproduced at least three times (biological replicates). The oligomycin-insensitive OCR (a measure of mitochondrial uncoupling) was determined after the addition of 2.5 μM oligomycin. The non-mitochondrial OCR that remained after the addition of rotenone/antimycin A (2 μM) was subtracted.

*Statistical analyses*–The results are presented as the means ± s.d. unless otherwise specified. The *P* values were calculated with Student`s t-test. Analysis of variance was performed for comparisons between more than two groups followed by a post-test (Tukey`s multiple comparison test unless otherwise specified), and statistical significance was set at a *P* value of <0.05 unless otherwise stated.

## RESULTS

*FASN-transgenic cardiomyocytes developed a dysfunctional cardiac substrate metabolism*–A dysfunctional cardiac substrate metabolism is a common feature of late-stage heart failure with limited treatment options. To reproduce the energy substrate use of heart failure patients and experimental models, which commonly show up-regulation of the major palmitate-synthesizing enzyme, *FASN* (10,11), we generated a transgenic model with myocardium-specific *FASN* expression under the control of the α-MHC-promoter (Fig. 1*A*, *B*). Immunoblot detection of the FASN protein confirmed transgenic protein expression in hearts from mice with stable genomic integration of the *FASN* transgene whereas the Fasn protein was barely detectable in non-transgenic B6 hearts (Fig. 1*C*). Two different transgenic lines (derived from founders no. 3 and 9) were established, which showed comparable FASN protein levels (Fig. 1*C*). All of the experiments were independently performed with these two transgenic lines.

After the generation of the transgenic mouse lines, the metabolic energetics of isolated neonatal *FASN*-transgenic (Tg-*FASN*) cardiomyocytes was determined with a Seahorse Bioscience XF24 Extracellular Flux Analyzer. We measured the β-oxidation of endogenous fatty acids by the Etomoxir-sensitive fraction of the oxygen consumption rate (OCR), and glycolysis by the 2-deoxyglucose-sensitive extracellular acidification rate (ECAR) (Fig. 1*D*, *E*). Compared to non-transgenic controls, *FASN*-transgenic cardiomyocytes showed significantly more β-oxidation under basal conditions (22.7±1.5% vs. 5.3±0.9%; Fig. 1*F*, *G*). This finding indicated that *FASN* increases the substrate availability of cardiomyocytes for β-oxidation.

We next determined the effect of an adult-like lipogenic milieu on neonatal cardiomyocytes by treatment with a 3F protocol consisting of insulin, IBMX, and dexamethasone for 10 days (23). In control cardiomyocytes, the 3F protocol switched the embryonic-like metabolism dominated by glycolysis (25) to an adult-like metabolism, which was characterized by an increased baseline OCR (Fig. 1*E*), and more fatty acid β-oxidation (Fig. 1*G*). In contrast, *FASN*-transgenic cardiomyocytes developed a heart failure-like phenotype with an overall depressed substrate metabolism (Fig. 1*E*), and predominant glycolysis (Fig. 1*F*). Thus, the increased availability of the lipid substrate, palmitate, did not protect neonatal cardiomyocytes from a substrate switch to a heart failure-like phenotype that had depressed bioenergetics dominated by glycolysis.

*FASN-transgenic mice developed signs of heart failure and cardiac lipid load*–The extracellular flux analysis detected a heart failure-like metabolic substrate use in isolated cardiomyocytes from Tg-*FASN* mice. But the method employs unloaded cardiomyocytes and does not represent the condition in the loaded myocardium, which functions with real heart rates. Therefore we analysed the cardiac phenotype in vivo. Our data show that adult *FASN*-transgenic mice developed signs of heart failure as early as 6 months of age, as evidenced by a significantly decreased left ventricular ejection fraction, cardiac hypertrophy with dilatation, and increased cardiomyocyte apoptosis (Fig. 2*A*-*E*). As a control,

the body weight of 6 month-old Tg-*FASN* mice was not different from B6 control mice (i.e., 34.28±1.02 g and 33.45±0.98 g, respectively; ±s.d.; n=4; *P*=0.5909).

The cardiac FASN protein in *FASN*-expressing mice was detected by immunoblotting and immunohistology (Fig. 2*F-H*). The FASN protein level in Tg-*FASN* hearts was increased ~2.4-fold (Fig. 2*F, G*), which is comparable to the up-regulated *FASN* level of failing human hearts (10,11).

Concomitantly to the increased FASN protein, cardiac free fatty acid (FFA) and triacylglycerol contents of Tg-*FASN* mice with signs of heart failure were elevated 2.2-fold and 2.1-fold, respectively (Fig. 2*I*, *J*). The cardiac contents of diacylglycerol (DAG) and ceramides, which can be induced by palmitate, i.e., the major lipid synthesized by *FASN*, were also significantly increased (Fig. 2*K, L*). These lipids could be involved in the heart failure phenotype of Tg-*FASN* mice because they trigger a wide spectrum of cardiotoxic mechanisms, which involves, e.g., the excessive formation of reactive oxygen species, an increased endoplasmic reticulum stress, enhanced apoptosis, and mitochondrial dysfunction (22,26). Additionally, increased cardiac contents of DAG and ceramide could mediate the activation of protein kinase C (PKC), which further decreases heart function (22,27,28). Thus, *FASN*-transgenic hearts developed signs of heart failure with cardiotoxic lipid load in addition to the dysfunctional energy substrate metabolism, which was detected in isolated cardiomyocytes.

*Up-regulation of the heart failure-related cardiac lipid metabolic process in FASN-transgenic mice*–Whole genome microarray gene expression profiling further confirmed the heart failure phenotype of Tg-*FASN* hearts by demonstrating the significant up-regulation of the heart failure-related cardiac lipid metabolic process (Fig. 3*A*). A similar induction of those adipogenic genes was also observed when signs of heart failure were triggered by 6 months of pressure overload (11) (Fig. 3*B*). In contrast, cardiac hypertrophy, without signs of heart failure (11) and induced by 4 weeks of pressure overload, did not up-regulate the heart failure-related adipogenic gene expression signature (Fig. 3*C*). Moreover, cardiac hypertrophy in the absence of heart failure signs promoted a significantly decreased expression of two probe sets that detect two enzymes of fatty acid biosynthesis, i.e., *Scd1* (Stearoyl-CoA desaturase-1) and *Acly* (ATP citrate lyase) (Fig. 3*C*). Thus, a heart failure-related adipogenic gene expression signature accompanied the onset of heart failure signs in *FASN*-transgenic mice.

*Heart failure-related adipogenic genes triggered by FASN are Pparg targets*–In search of *FASN*-induced pathomechanisms, we focused on the adipogenic and heart failure-promoting transcription factor, *Pparg* (29,30), because (i) palmitate, the major lipid synthesised by *FASN*, enhances the activity of *Pparg* (31), and (ii) adipogenic genes induced by *FASN* are *Pparg* targets (32), which are similarly up-regulated by *Pparg* over-expression in the mouse heart (29). Similarly, the treatment of ApoE-/- mice for 2 months with the *Pparg* agonist, rosiglitazone, also significantly up-regulated those heart failure-related adipogenic *Pparg* target genes, which were induced by *FASN* (Fig. 3*D*). As a control, rosiglitazone promoted signs of heart failure in ApoE-/- mice (cf. Fig. 4*F-I*). These findings demonstrate that the heart failure-related adipogenic gene signature induced by Tg-*FASN* and chronic pressure overload is also triggered by direct *Pparg* activation with rosiglitazone.

*Down regulation of endogenous Fasn reveals a causal relationship between Fasn and Pparg activation in promoting cardiac dysfunction*–Next we investigated the impact of *Fasn* on *Pparg*-induced cardiac dysfunction, and we knocked down the endogenously expressed *Fasn* by RNAi in rosiglitazone-treated ApoE-/- mice. Inhibition of *Fasn* by lentiviral transduction of a *Fasn*-specific miRNA (Fig. 4*A-D*) retarded the development of rosiglitazone-induced cardiac lipid load (Fig. 4*E*) and signs of rosiglitazone-induced heart failure (Fig. 4*F-I*). Together these data confirmed the causal relationship between *Fasn* and enhanced *Pparg* activation in promoting cardiotoxicity and cardiac dysfunction.

*GRK2 inhibition by GRKInh in FASN-transgenic mice*–In view of the central role of *FASN*, the inhibition of *FASN* would be a straightforward treatment approach. However, *FASN* is an essential enzyme that has indispensable functions in energy homeostasis, membrane biology and neurogenesis, which preclude long-term *FASN* inhibition in vivo (10,33,34). We therefore searched for an alternative strategy to target the dysfunctional

cardiac substrate metabolism. We focused on the inhibition of GRK2, which is a well-established means of cardioprotection (12,35). Furthermore, GRK2 inhibition enhances the ERK cascade (12), which promotes (partial) inactivation of *Pparg* (36). In agreement with heart failure patients (37), the GRK2 protein levels were significantly up-regulated (i.e., 1.81±0.12-fold) in Tg-*FASN* hearts with signs of heart failure relative to the B6 controls (Fig. 5*A*).

To inhibit GRK2 in vivo, we used a GRK2-specific inhibitor peptide (GRKInh) derived from the first intracellular loop of the β2 adrenergic receptor (12,17). We used transgenic mice with myocardium-specific expression of GRKInh, which were established previously (12). The GRKInh peptide interacted specifically with GRK2 in heart tissue extracts from Tg-GRKInh/*FASN* mice as demonstrated by co-enrichment whereas the amount of GRK5 co-enriched with GRKInh-specific antibodies was below the limit of detection (Fig. 5*B*). Quantitative assessment of the GRK2-GRKInh interaction indicated that 83.6±4.2 % of the total cardiac GRK2 protein was captured by GRKInh-affinity enrichment whereas the amount of GRK5 protein bound to GRKInh was less than 20% (i.e., 18.9±2.2%) of the total cardiac GRK5 content (Fig. 5*C*).

The functional effects of GRK2 inhibition in transgenic Tg-GRKInh/*FASN* hearts were analyzed by the immunofluorescence detection of Arrb1, which translocates to phosphorylated membrane-spanning receptors as a direct consequence of GRK2-mediated phosphorylation (Fig. 5*D*). In agreement with an increased GRK2 activity, immunofluorescence analysis detected the substantial membrane localization of Arrb1 in a cardiac section from a Tg-*FASN* mouse with signs of heart failure (Fig. 5*D*, left). In contrast, the double-transgenic Tg-GRKInh/*FASN* heart section showed a largely cytoplasmic localization of Arrb1 as evidenced by co-localization with the cytosolic p38 MAPK (Fig. 5*D*, right). These findings indicate that GRKInh interacts with GRK2 in hearts from double-transgenic Tg-GRKInh/*FASN* mice. As a consequence of the GRKInh-GRK2 interaction, the enhanced GRK2-mediated Arrb1 membrane translocation could be blunted.

*GRK2 inhibition by GRKInh prevents the dysfunctional cardiac energetics of FASN-transgenic cardiomyocytes*–We characterised the substrate metabolism of isolated neonatal cardiomyocytes from double-transgenic Tg-GRKInh/*FASN* mice compared to single-transgenic Tg-*FASN* mice. Under basal conditions, the presence of GRKInh retarded the premature appearance of an adult-like metabolic phenotype with an increased baseline OCR of Tg-*FASN* cardiomyocytes (Fig. 6*A*, *B*). Concomitantly, the increased β-oxidation of Tg-*FASN* cardiomyocytes under basal conditions was also retarded in double-transgenic Tg-GRKInh/*FASN* cardiomyocytes (Fig. 6*A*, *C*). Notably, the extent of β-oxidation of Tg-GRKInh/*FASN* double-transgenic cardiomyocytes was not significantly different from that of the B6 control, i.e., 6.0±1.0 % vs. 5.4±1.7%, respectively (Fig. 6*A*, *C*). Moreover, under the 3F protocol, GRKInh retarded the shift to a heart failure-like metabolic phenotype of Tg-*FASN* cardiomyocytes, which is characterized by predominant glycolysis and decreased β-oxidation (Fig. 6*A*, *B* and Fig. 6*C*-*E*). Similarly to non-transgenic B6 controls, the Tg-GRKInh/*FASN* cardiomyocytes shifted to an adult-like phenotype, which is characterised by an increased baseline OCR and an elevated β-oxidation (Fig. 6*A*, *B* and Fig. 6*C*-*E*).

The improved metabolic profile of Tg-GRKInh/*FASN* cardiomyocytes was accompanied by a resensitization of adiponectin receptor protein 1 (*Adipor1*)-mediated signalling (Fig. 6*F*), which is desensitized by GRK2 in the ischemic heart (14). Notably, the inhibition of GRK2 in Tg-GRKInh/*FASN* cardiomyocytes led to a significantly increased protein level of activated phospho-Prkaa upon adiponectin stimulation whereas the adiponectin-stimulated signal was largely blunted in Tg-*FASN* cardiomyocytes (Fig. 6*F*). This finding could be relevant because *Adipor1* and its target AMP-activated protein kinase (*Prkaa*) could protect against palmitate-induced toxicity (15,16).

*GRK2 inhibition retards the development of heart failure signs in Tg-FASN mice*–The improved substrate metabolism upon GRK2 inhibition was also reflected in vivo, in adult murine hearts. The presence of GRKInh in double-transgenic Tg-GRKInh/*FASN* hearts compared to single-transgenic Tg-*FASN* hearts led to a significantly decreased total FFA and triacylglycerol load compared to single-transgenic Tg-*FASN* hearts (Fig. 7*A*, *B*).

The decreased lipid load of Tg-GRKInh/*FASN* hearts was accompanied by a significantly decreased cardiac expression of the acetyl-CoA carboxylase alpha (*Acaca*), which mediates an essential step of fatty acid synthesis by catalysing the conversion of acetyl-CoA into malonyl-CoA (Fig. 7*C*). Notably, GRKInh largely prevented the up-regulation of *Acaca,* i.e., a gene up-regulated by hypoxia (38), which was commonly triggered at the onset of heart failure induced by Tg-*FASN*, pressure overload and *Pparg* (Fig. 7*C* and cf. Fig. 3*A*, *B*, *D*).

Although the expression of the human *FASN* transgene was not significantly altered between single-transgenic Tg-*FASN* and double-transgenic Tg-GRKInh/*FASN* hearts (Fig. 7*D*, left panel), GRKInh led to a significantly decreased expression of the endogenous murine *Fasn* gene, which is also a hypoxia-induced *Pparg* target (39), and shows up-regulated expression in Tg-*FASN* hearts with signs of heart failure (Fig. 7*D*, right panel, and cf. Fig. 3*A*). Concomitantly, the total cardiac FASN/Fasn protein level of Tg-GRKInh/*FASN* hearts was significantly decreased relative to that in Tg-*FASN* hearts (Fig. 7*E*). Together these experiments show that GRK2 inhibition retards the *FASN*-induced dysfunction of the cardiac substrate metabolism and lipid overload. Concomitantly with the decreased lipid load, the development of signs of heart failure such as cardiac dysfunction, cardiac hypertrophy, cardiac ATP depletion and *FASN/Fasn*-mediated cell death, was significantly retarded (Fig. 7*F*-*I*).

*GRK2 inhibition promotes ERK axis-dependent inhibition of Pparg transcriptional activity*–We investigated the mechanism that accounts for GRK2 inhibition-mediated protection against *FASN*-induced cardiolipotoxicity, and focused on the interrelationship between GRK2 inhibition-mediated ERK axis activation and the inactivation of *Pparg*. Several lines of evidence support such a relationship. (i) The expression of several heart failure-related *Pparg* targets such as adiponectin (*Adipoq*), resistin (*Retn*) and uncoupling protein 1 (*Ucp1*), is down-regulated by ERK-dependent inactivation of *Pparg*, partially by involving serine-273 phosphorylation (36,40). (ii) GRK2 inhibition enhances the activation of the ERK cascade (12,41). (iii) Additionally, the reversal of palmitate toxicity can be achieved by ERK activation, e.g., triggered by AMPK signalling (16), i.e., the signalling pathway that was re-sensitised by GRK2 inhibition (cf. Fig. 6*F*). Conversely, excess palmitate down-regulated the ERK axis (16).

In agreement with palmitate-mediated inhibition of ERK (16), the cardiac content of activated phospho-ERK1/2 was low in Tg-*FASN* hearts relative to double-transgenic Tg-GRKInh/*FASN* hearts (Fig. 7*J*, *K*). Notably, GRKInh enhanced the activation of ERK2 (Fig. 7*K*), which is cardioprotective and protects the myocardium against ischemic injury (42). Concomitantly with enhanced ERK1/2 activation, serine-273 phosphorylated *Pparg* was increased in double-transgenic Tg-GRKInh/*FASN* hearts relative to Tg-*FASN* hearts (Fig. 7*L*).

In agreement with the ERK-dependent inactivation of *Pparg* (36,40,43), the enhanced phosphorylation of *Pparg* on serine-273 and serine-112 of double-transgenic Tg-GRKInh/*FASN* cardiomyocytes was accompanied by a significantly decreased *Pparg* transcription factor DNA-binding activity compared to that of Tg-*FASN* cardiomyocytes (Fig. 7*M*, *N*). The decreased *Pparg* activity of Tg-GRKInh/*FASN* cardiomyocytes was dependent on an activated ERK axis because the MEK inhibitor PD0325901 blunted the phosphorylation of *Pparg* on serine-273 and serine-112, and led to a significant up-regulation of the *Pparg* transcriptional activity of Tg-GRKInh/*FASN* cardiomyocytes (Fig. 7*M*, *N*).

Concomitantly with *Pparg* inhibition, the expression of ERK-regulated, heart failure-related *Pparg* targets (i.e., *Ucp1*, *Adipoq*) was significantly lower in double-transgenic Tg-GRKInh/*FASN* hearts compared to Tg-*FASN* hearts (Fig. 7*O*). Concordantly with decreased signs of heart failure, GRKInh also led to a significantly decreased expression of the heart failure marker and *Pparg* target gene, resistin (*Retn*) (Fig. 7*O*). Because *Adipoq* and *Retn* are heart failure-related *Pparg* targets (44,45) that are induced by serine-273 phosphorylation-deficient *PPARG-S273A* (40), these data are compatible with the notion that cardioprotective GRK2 inhibition could involve the suppression of *Pparg*-dependent cardiolipotoxic gene expression by enhanced ERK-mediated serine-273 phosphorylation and the inactivation of *Pparg*.

*Inhibition of Fasn lowers the cardiolipotoxicity induced by serine-273 phosphorylation-deficient PPARG-S273A*–We analysed the impact of phosphorylation-deficient

*PPARG-S273A* on cardiomyocyte function. Our experiments showed that both cardiomyocyte FFA content and the Fasn protein were triggered by *PPARG* activated with the *PPARG* agonist rosiglitazone and by *PPARG-S273A* (Fig 8*A*, *C*, *D*). These data are in agreement with those from previous studies, which have shown that *PPARG* serine-273 dephosphorylation can enhance the expression of Fasn (46).

Concomitantly with the FFA load, cardiomyocyte dysfunction developed as evidenced by a significantly decreased cardiomyocyte ATP content induced either by rosiglitazone-activated *PPARG* or *PPARG-S273A*, respectively (Fig. 8*B*). The inhibition of *Fasn* by RNAi (Fig. 8*C*, *D*) led to significantly decreased cardiomyocyte FFA content and largely prevented the decrease in cardiomyocyte ATP (Fig. 8*A*, *B*). Together these findings provide evidence that *PPARG-S273A* deteriorates cardiomyocyte function by regulating *Fasn*.

*GRK2 inhibition retards the up-regulation of the heart failure-related Ucp1 and mitochondrial uncoupling*–In search of additional heart failure-promoting ERK-controlled *Pparg* target genes, we focused on *Ucp1* (36,47), which exerts mitochondrial uncoupling, a major metabolic feature of the failing heart metabolism (9). GRK2 inhibition by GRKInh led to a decreased cardiac *Ucp1* expression and protein level in Tg-GRKInh/*FASN* mice relative to Tg-*FASN* mice (Fig. 9*A* and cf. Fig. 7*O*). Moreover, cardiomyocytes from Tg-GRKInh/*FASN* mice showed a significantly decreased oligomycin-insensitive OCR (a measure of mitochondrial uncoupling) compared to Tg-*FASN* cardiomyocytes (Fig. 9*B*). Conversely, the inhibition of the ERK axis in Tg-GRKInh/*FASN* cardiomyocytes significantly increased the *Ucp1* protein and mitochondrial uncoupling (Fig. 9*B*, *C*). These findings indicate that GRK2 inhibition decreased *Ucp1*-dependent mitochondrial uncoupling in Tg-GRKInh/*FASN* cardiomyocytes by enhanced activation of the ERK axis.

*Transgenic Tg-UCP1 mice developed signs of heart failure and increased mitochondrial uncoupling*–To analyse whether an increased cardiac *UCP1* level contributed to heart failure pathogenesis in vivo, we generated Tg-*UCP1* mice with myocardium-specific *UCP1* expression (Fig. 10*A*, *B*). Immunoblot detection confirmed the increased cardiac UCP1 protein in Tg-*UCP1* (Tg-6) mice relative to non-transgenic B6 controls (Fig. 10*C*). In addition to the Tg-6 line, we also used Tg-11 offspring with lower UCP1 protein levels (Fig. 10*D*).

Aged Tg-*UCP1* mice from the Tg-6 line developed cardiac dysfunction with a significantly decreased left ventricular ejection fraction and decreased cardiac ATP content compared to non-transgenic B6 mice whereas cardiac function parameters of the low-expressing Tg-11 line were not significantly different from B6 controls (Fig. 10*E*, *F*). Concomitantly with cardiac dysfunction, Tg-*UCP1* mice showed cardiac dilatation and loss of heart muscle, whereas the heart-weight-to-body-weight ratio was not significantly different from that in the B6 controls (Fig 10*G*, *H*). Signs of heart failure were accompanied by a significant up-regulation of the cardiac Fasn protein in Tg-*UCP1* mice compared to non-transgenic B6 controls (Fig. 10*I*). The up-regulation of the Fasn protein by *UCP1* could be a consequence of the impaired cardiac function and insufficient tissue oxygen supply, which could induce *Fasn* up-regulation because it is a hypoxia-induced gene (39).

The ensuing increase in palmitate may enhance mitochondrial uncoupling by the transgenic UCP1 protein. In support of that notion, Tg-*UCP1* cardiomyocytes showed a significantly increased oligomycin-insensitive (uncoupled) respiration compared to B6 cardiomyocytes (Fig. 10*J*). Together these experiments indicate that the UCP1 protein could have a major role in the depressed substrate metabolism of a failing heart because up-regulated UCP1 could account for an enhanced palmitate-triggered uncoupled respiration upon *FASN* induction. Under those conditions, GRK2 inhibition by GRKInh could confer several modes of cardioprotection: (i) By counteracting mitochondrial uncoupling via ERK activation-mediated down-regulation of *UCP1* (36); and (ii) by decreasing the *FASN*-triggered lipid load, which involves, e.g., down-regulation of hypoxia-induced *Pparg* targets, *Acaca* and *Fasn*, and the resensitisation of *Prkaa*.

*Inhibition of Ucp1 counteracts PPARG-S273A-induced cardiolipotoxicity*–The mechanism of ERK-mediated down-regulation of the *Pparg* target, *Ucp1*, is not completely understood (36,47). *Ucp1* is a *Pparg* target that is highly up-regulated in Tg-*FASN* and pressure overload-induced heart failure models, and by direct *Pparg* activation with

rosiglitazone (cf. Fig. 3). Low ERK axis activity in these models could mediate stabilization of transcriptional cofactors that are necessary for *Ucp1* induction, i.e., *PGC1a* or *PRDM16* (36). Moreover, recent data have shown that *PPARG-S273* dephosphorylation can also enhance the recruitment of *PGC1a* as a transcriptional cofactor involved in *Ucp1* induction (46). To analyse the interplay between *Ucp1* and *PPARG-S273A*-mediated cardiolipotoxicity, we inhibited *Ucp1* by RNAi. The inhibition of *Ucp1* led to an increased ATP content of cardiomyocytes with rosiglitazone-activated *PPARG* and with *PPARG-S273A* expression, while concomitantly decreasing the cardiomyocyte FFA content (Fig. 10*K*). These findings obtained with *Ucp1* are analogous to the data obtained with *Ucp2*, which showed that (i) the *Ucp2* knockout decreased the cellular lipid content of pancreatic islets as a consequence of higher palmitate oxidation (48); and (ii), *Ucp1* knockdown attenuated the free fatty acid-induced apoptosis of cardiomyocytes (49); and (iii), conversely, *Ucp2* overexpression decreased the cardiomyocyte ATP levels (50). Taken together, the data are compatible with the notion that *Ucp1* exerts a detrimental role in cardiolipotoxicity, as triggered, e.g., by *Pparg* activation with rosiglitazone and/or serine-273 dephosphorylation. However, the inhibition of *Ucp1* could counteract such cardiotoxic effects.

*Cardioprotective GRK2 inhibition requires an intact ERK axis*–We further investigated the impact of ERK activation on cardioprotective GRK2 inhibition and applied the dual-specific GRK2 and ERK cascade inhibitor, RKIP (21). RKIP-transgenic mice with myocardium-specific expression of the human RKIP (*PEBP1*) were previously generated and characterised (12). RKIP-transgenic and GRKInh-transgenic hearts display similar inhibition of GRK2 (12). Similarly, isolated neonatal cardiomyocytes of RKIP-transgenic and GRKInh-transgenic mice showed a comparable enhancement of the isoproterenol-stimulated cAMP response (Fig. 11*A*). This observation confirmed that the two different GRK2 inhibitors were expressed at equivalent levels with regard to the sensitization of the β-adrenergic receptor response. However, in contrast to GRKInh, transgenic hearts that expressed the dual-specific GRK2/ERK cascade inhibitor, RKIP, were characterised by a significantly decreased phosphorylation of *Pparg* on serine-273 (Fig. 11*B*, *C*), which is ERK dependent (36).

We next determined the expression of cardiac *Pparg* targets of RKIP-transgenic hearts because the inhibition of *Pparg* serine-273 phosphorylation induces *Pparg* target gene expression (36). Gene expression analysis revealed the significant up-regulation of heart failure-related *Pparg* targets (Fig 11*D*). Some of those highly up-regulated heart failure genes, such as adipsin (*Adn*), adiponectin (*Adipoq*), fatty acid synthase (*Fasn*), resistin (*Retn*), and uncoupling protein-1 (*Ucp1*), are reportedly induced by the inhibition of ERK and/or serine-273 dephosphorylation of *Pparg* (36,40,46), which was triggered by RKIP (cf. Fig. 11*B*, *C*). In agreement with heart failure-related adipogenic target gene up-regulation, cardiac lipid load developed, and cardiac dysfunction became evident in hearts of aged RKIP-transgenic mice (Fig. 11*E-H*; and ref. 12). In vitro data documented the dysfunctional cardiomyocyte energetics of RKIP-transgenic cardiomyocytes compared to the normal metabolism of GRKInh-transgenic cardiomyocytes (Fig. 11*I-M*). Taken together our data strongly suggest that an intact ERK axis is required for GRK2 inhibition-dependent protection against dysfunctional metabolic substrate use.

*GRK2 inhibition retards the development of heart failure signs, cardiac lipid load and Pparg target gene induction in a pressure overload-induced heart failure model*–Thus, we have presented evidence for GRKInh-mediated protection of Tg-*FASN* hearts. However, up-regulation of the *Pparg*-dependent lipid metabolic process is also a characteristic feature of heart failure models that imitate major risk factors of patients such as chronic pressure overload (cf. Fig 3*B* and ref. 11). We therefore analysed the effect of GRKInh on the cardiac lipid metabolism in a chronic pressure overload-induced heart failure model imposed by long-term (6 months) abdominal aortic constriction, AAC.

In agreement with previous data (12), AAC promoted cardiac hypertrophy with dilatation in non-transgenic mice, whereas Tg-GRKInh mice showed a significantly decreased cardiac hypertrophy (Fig. 12*A*, *B*). The development of cardiac dysfunction upon AAC, as assessed by the left ventricular ejection fraction, was also significantly retarded in Tg-GRKInh

mice (Fig. 12*C*). In addition to the improved cardiac function, the AAC-stimulated up-regulation of the cardiac Fasn protein was blunted in Tg-GRKInh mice (Fig. 12*D*). Concomitantly, oil red O staining of cardiac sections indicated that the AAC-triggered lipid load was lower in Tg-GRKInh mice (Fig. 12*E*). In agreement with the decreased lipid-induced cardiolipotoxicity, Tg-GRKInh mice showed a significantly decreased number of AAC-induced TUNEL-positive cardiomyocytes compared to the number in non-transgenic mice with AAC (Fig. 12*F*, *G*).

In view of the decreased AAC-induced cardiolipotoxicity, we analysed the potential effect of GRK2 inhibition on *Pparg*-inhibitory serine-273 phosphorylation. Immunoblot detection indicated an increased cardiac content of serine-273-phosphorylated *Pparg* of Tg-GRKInh hearts with AAC compared to non-transgenic B6 mice with AAC (Fig. 12*H*, *I*). The increased level of *Pparg*-inhibitory serine-273 phosphorylation was accompanied by a significantly lower expression of heart failure-related *Pparg* targets, which are blunted by ERK activation and/or ERK-dependent *Pparg* serine-273 phosphorylation, i.e., *Ucp1*, *Adipoq* and *Retn* (Fig. 12*J*). Taken together, cardioprotective GRK2 inhibition with GRKInh retarded the up-regulation of heart failure-related and ERK-inhibited *Pparg* targets, and enhanced *Pparg*-inhibitory serine-273 phosphorylation.

*Down-regulation of endogenous Ucp1 retards the development of cardiac dysfunction in a pressure overload-induced heart failure model*–Although previous studies have provided evidence for the involvement of *Adipoq* and *Retn* in heart failure pathogenesis of patients and animal models (44,45,51-53), the role of *Ucp1* up-regulation in cardiac dysfunction is less clear. Notably, the onset of heart failure signs in different heart failure models was characterised by a strong cardiac *Ucp1* up-regulation (cf. Fig. 3), and transgenic expression of *UCP1* in the heart promoted signs of heart failure (cf. Fig. 10). To investigate the effect of *Ucp1* up-regulation in the AAC-induced heart failure model, we down-regulated the endogenously expressed *Ucp1* by lentiviral transduction of an miRNA that targets *Ucp1* by RNA interference (Fig. 13*A,B*). The down-regulation of *Ucp1* in the AAC-induced heart failure model led to a small, but significant retardation of the development of AAC-induced cardiac dysfunction (Fig. 13*C*). These findings provide further evidence (cf. Fig. 10) for the role of *Ucp1* up-regulation in AAC-induced signs of heart failure.

*Low efficacy of GRKInh in retarding the cardiac phenotype of PPARG-S273A-transgenic mice*–Our data provided evidence that GRK2 inhibition counteracts the dysfunctional cardiac substrate use of heart failure (at least partially) by ERK-dependent inactivation of *Pparg* involving serine-273 phosphorylation. To further analyze the role of *PPARG* and a serine-273 phosphorylation-deficient *PPARG* mutant (PPARG-S273A) in the heart, we generated transgenic mice with myocardium-specific expression of wild-type *PPARG* and mutated *PPARG*-S273A, respectively (Fig. 14*A*). Histological analysis revealed that transgenic *PPARG*-S273A mice developed cardiac hypertrophy with dilatation, which was already evident in newborn mice (Fig. 14*B*). The dilatation of the *PPARG*-S273A-expressing heart was greater than that of the *PPARG*-expressing heart (Fig. 14*B*), although the cardiac PPARG protein level was comparable between the two transgenic groups (Fig. 14*C*).

Next we investigated the effect of GRK2 inhibition by GRKInh, and compared single transgenic mice (*PPARG*-S273A and *PPARG*), with double-transgenic *PPARG*-S273A+GRKInh-expressing and *PPARG*+GRKInh-expressing mice, respectively. All 4 groups of mice showed similar cardiac *PPARG* expression (Fig. 14*D*). Despite of having similar *PPARG* expression, the GRKInh largely prevented the cardiac hypertrophy of *PPARG*-expressing mice, whereas the effect of GRKInh on *PPARG*-S273A-expressing mice was not significant (Fig. 14*E*). In addition, there was an increased postnatal mortality of *PPARG*-S273A-expressing mice compared to wild-type *PPARG*-expressing mice (47.8.% vs. 9.5 %), which was not rescued by the GRK2 inhibitor (Fig. 14*F*).

We determined the expression of selected heart failure-related *Pparg* targets, i.e., *Adipoq*, *Retn*, *Fasn* and *Ucp1*. The genes were all significantly up-regulated in the cardiac tissue of four week-old *PPARG*-S273A-transgenic mice compared to non-transgenic B6 mice (Fig. 14*G*), which confirms the heart failure-like phenotype of newborn *PPARG*-S273A transgenic mice. We found that the effect of GRKInh was not significant in reducing the *PPARG*-S273A-mediated up-regulation of *Adipoq*, *Retn*, *Fasn* and

*Ucp1* (Fig. 14*G*). In contrast to *PPARG*-S273A-transgenic hearts, the transgenic expression of *PPARG* caused significantly less up-regulation of selected *Pparg* targets, and only the expression of cardiac *Adipoq* and *Fasn* was significantly increased in four week-old mice (Fig. 14*G*). The up-regulation of *Adipoq* in *PPARG*-transgenic mice may have contributed to the cardiac hypertrophy (cf. Fig. 14*B*, *E*) because *Adipoq* is required for pro-hypertrophic signaling during pressure overload (44).

In agreement with the heart failure-like phenotype of *PPARG*-S273A-expressing mice, the cardiomyocyte energetics of neonatal cardiomyocytes from *PPARG*-S273A-transgenic mice showed an overall depressed substrate metabolism under basal conditions with predominant glycolysis. This heart failure-like substrate use was not rescued by co-expression of GRKInh (Fig. 14*H*). Conversely, *PPARG*-expressing cardiomyocytes showed predominant β-oxidation under basal conditions indicative of lipid load, which was retarded by GRKInh (Fig. 14*H*). Upon induction of an adult-like metabolism by the 3F protocol, *PPARG*-expressing cardiomyocytes shifted to a heart failure-like metabolic substrate use (Fig. 14*H*). In contrast to *PPARG*-S273A, the development of the *PPARG*-induced heart failure-like phenotype was retarded by GRKInh (Fig. 14*H*). Together these findings provide evidence for an enhanced cardiac deterioration of *PPARG*-S273A-transgenic mice compared to *PPARG*-WT mice. Moreover, GRKInh was inefficient in retarding the development of the *PPARG*-S273A-induced cardiometabolic dysfunction and the up-regulation of *PPARG*-S273A-regulated targets.

## DISCUSSSION

In the present study we investigated whether GRK2 inhibition could be a specific approach for targeting of the dysfunctional cardiac substrate metabolism, which is characteristic of late-stage heart failure (4-6). To reproduce the dysfunctional cardiac substrate use, we generated a novel transgenic model with myocardium-specific *FASN* expression. The model imitated the up-regulation of *FASN*, which occurs in patients with heart failure (10,11). In the context of cardiovascular disease and heart failure, the up-regulation of *FASN* could be a direct consequence of decreased cardiac output and insufficient oxygen supply because *FASN* is a hypoxia-induced gene (39). Because cardiac ischemia is triggered by major cardiovascular risk factors such as pressure overload and atherosclerosis, up-regulation of *FASN* could also be an early and causative event in the pathogenesis of heart failure. In agreement with this notion, we found that the sole expression of *FASN* was sufficient to trigger the signs of heart failure. Additionally, models of heart failure, which imitated cardiovascular risk factors of patients such as chronic pressure overload or advanced atherosclerosis, also showed up-regulation of cardiac Fasn (11).

How could *FASN* advance the symptoms of heart failure? Initially, up-regulation of *FASN* might be considered to be beneficial by supplying more energy substrate to the heart muscle. However, in the long-term, the uncontrolled accumulation of palmitate as the major lipid synthesised by *FASN* could activate the heart failure-promoting transcription factor *Pparg*, as has been documented by up-regulation of the *Pparg*-dependent lipid metabolic process in Tg-*FASN* hearts and various other models of heart failure. Because *Fasn* is also a *Pparg* target, a vicious cycle of *FASN/Fasn*-induced *Fasn* could be triggered, which finally results in cardiotoxic lipid load, dysfunctional substrate use and mitochondrial uncoupling due to palmitate-triggered activation of *Ucp1* (Fig. 15). The accumulation of palmitate further promotes pro-apoptotic signalling and inhibits the pro-survival ERK axis (16). As a result, there is an enhanced expression of heart failure-associated *Pparg* targets that are triggered by ERK inhibition (36,40), such as *Adipoq* (44,51,52), *Retn* (45,53), and *Ucp1*. Ensuing cardiomyocyte death and remodelling, and impaired cardiac energy generation due to mitochondrial uncoupling could further aggravate the symptoms of heart failure (Fig. 15).

When we applied the Tg-*FASN* mice as a model of a dysfunctional cardiac substrate metabolism and an additional pressure overload-induced heart failure model, we found that GRK2 inhibition directly interfered with the cardiac lipid accumulation and mediated a reduction in the cardiac Fasn protein. These activities could be attributed (at least partially) to several mechanisms: (i) the inhibition of the endogenous *Fasn* up-regulation, a hypoxia-induced *Pparg*

target (39), (ii) an interference with fatty acid synthesis by preventing *Acaca* up-regulation, which is also a *Pparg*-regulated gene induced by hypoxia (38), and (iii) the enhancement of the fatty acid metabolism by re-sensitisation of *Adipor1* and *Prkaa*-mediated signalling (14). As a consequence, GRK2 inhibition retarded the development of the dysfunctional cardiac substrate use characteristic of late-stage heart failure (Fig. 15).

Cardioprotective GRK2 inhibition required an intact ERK axis to preserve the cardiac energetics because RKIP as a dual-specific GRK2 and ERK cascade inhibitor promoted dysfunction of cardiomyocyte energetics, cardiac lipid load and signs of heart failure. Concomitantly, inhibition of the ERK cascade by human RKIP was accompanied by decreased ERK-dependent phosphorylation of *Pparg*. A decreased ERK-dependent phosphorylation of *Pparg* on serine-273 and serine-112 is known to enhance *Pparg* activity and/or increase *Pparg* target gene induction (36,40,43). Similarly, heart failure-related *Pparg* targets are triggered by RKIP, resulting in development of cardiac lipid load and cardiac dysfunction (12).

Conversely, GRK2 inhibition by GRKInh led to an increased ERK activation and enhanced the ERK-mediated phosphorylation of *Pparg* on serine-273. ERK axis activation could be part of the cardioprotective gene expression program initiated by GRK2 inhibition (12,13,41). Concomitantly, the expression of heart failure-promoting *Pparg* targets was blunted, and the appearance of the dysfunctional cardiac substrate metabolism was retarded. In agreement with a causal role of *PPARG*-S273 phosphorylation in GRKInh-mediated cardioprotection, the phosphorylation-deficient *PPARG*-S273A mutant promoted dysfunction of the cardiomyocyte substrate metabolism and caused enhanced postnatal death, which was largely insensitive to GRKInh. In contrast, the phenotype of wild-type *PPARG* was less severe and could be (at least partially) rescued by GRK2 inhibition. Together these data indicate that the ERK axis may specifically counteract the heart failure-promoting transcription factor *Pparg* by preventing heart failure-related *Pparg* target gene induction (36,54) and/or could confer protection against palmitate-induced endoplasmic reticulum stress (55).

Several heart failure-related *Pparg* targets are inhibited by ERK-dependent *Pparg* inactivation (36,40) with GRKInh, such as *Adipoq* (44,51,52) and *Retn* (45,53). By generating Tg-*UCP1* mice with myocardium-specific *UCP1* expression, our study identified *UCP1* as a heart failure-related ERK-regulated *Pparg* target (36,47), which was also down-regulated upon GRK2 inhibition (Fig. 15). Consequently, GRK2 inhibition could decrease excessive mitochondrial uncoupling as a key event that contributes to inefficient cardiac ATP generation and lipid-induced cardiomyocyte death in heart failure (49,50).

Although the study was performed with experimental mouse models, the data could also be relevant for the human disease because *FASN* up-regulation is a characteristic feature of patients with heart failure (10,11). Because *PPARG* up-regulation occurs in heart failure patients with pressure-overloaded heart and metabolic syndrome (56), GRK2 inhibition is expected to disrupt a vicious *FASN*/*PPARG* cycle in patients who suffer from multiple risk factors (Fig. 15). Such a situation was modelled with rosiglitazone-treated ApoE-/- mice because these mice are prone to the development of atherosclerosis and insulin resistance (57), and thereby mimic the risk profile of patients with enhanced *PPARG* activation and cardiovascular disease. In this model, *Pparg* activation triggered the up-regulation of *Fasn* and signs of heart failure within two months. The causal interplay between *Fasn* and *Pparg*-induced cardio-toxicity was demonstrated by RNAi-mediated inhibition of *Fasn,* which prevented the *Pparg*-induced cardio-lipotoxicity and signs of heart failure. Because GRK2 inhibition also mediated the down-regulation of *FASN*-dependent cardio-lipotoxicity, patients with high morbidity and multiple risk factors may benefit from GRK2 inhibition. The additional insulin sensitivity-enhancing activity of GRK2 inhibition (13,58) may further increase the value of such a strategy.

Moreover, heart-specific GRK2 inhibition could become a cardioprotective combination partner for a novel class of insulin sensitivity-enhancing *PPARG* activators, which rely on the inhibition of ERK-dependent *PPARG* phosphorylation for antidiabetic activity (36), but have promoted signs of heart failure in clinical trials (59).

In sum, our study provides strong evidence that cardioprotective GRK2 inhibition specifically targets the dysfunctional cardiac substrate use that is a symptom of late-stage heart failure (Fig. 15). The identified targeting approach could stimulate the development of new therapeutic strategies.

**Acknowledgments:** We thank James Gulick for the Alpha-MyHC plasmid.

**Conflict of interest:** The authors declare that they have no conflict of interest with the content of this article.

**Author contributions:** J.A., M.G. and U.Q. analysed the data and produced all of the figures. J.A. and X.F. generated the transgenic mice. J.A. and U.Q. wrote the main manuscript text. All of the authors reviewed the results and approved the final version of the manuscript.



**REFERENCES**

1. Nakou, E. S., and Vardas, P. E. (2013) New therapeutic options in heart failure. What`s on the horizon? An overview. *Int. J. Cardiol.* **170**, 95-106
2. Bu, A. L., Horwich, T. B., and Fonarow, G. C. (2011) Epidemiology and risk profile of heart failure. *Nat. Rev. Cardiology* **8**, 30-41
3. Taegtmeyer, H., and Stanley, W. C. (2011) Too much or not enough of a good thing? Cardiac glucolipotoxicity versus lipoprotection. *J. Mol. Cell. Cardiol.* **50**, 2-5
4. Wittels, B., and Spann, J. F. (1968) Defective lipid metabolism in the failing heart. *J. Clin. Invest.* **47**, 1787-1794
5. Bishop, S. P., and Altschuld, R. A. (1970) Increased glycolytic metabolism in cardiac hypertrophy and congestive failure. *Am. J. Physiol.* **218**, 153-159
6. Stanley, W. C., Recchia, F. A., and Lopaschuk, G. D. (2005) Myocardial substrate metabolism in the normal and failing heart. *Physiol. Rev.* **85**, 1093-1129
7. Berthiaume, J. M., Bray, M. S., McElfresh, T. A., Chen, X., Azam, S., Young, M. E., Hoit, B. D., and Chandler, M. P. (2010) The myocardial contractile response to physiological stress improves with high saturated fat feeding in heart failure. *Am. J. Physiol. Heart Circ. Physiol.* **299**, H410-H421
8. Lahey, R., Wang, X., Carley, A. N., and Lewandowski, E. D. (2014) Dietary fat supply to failing hearts determines dynamic lipid signaling for nuclear receptor activation and oxidation of stored triglyceride. *Circulation* **130**, 1790-1799
9. Neubauer, S. (2007) The failing heart - an engine out of fuel. *N. Engl. J. Med.* **356**, 1140-1151
10. Razani, B., Zhang, H., Schulze, P. C., Schilling, J. D., Verbsky, J., Lodhi, I. J., Topkara, V. K., Feng, C., Coleman, T., Kovacs, A., Kelly D. P., Saffitz, J. E., Dorn G. W., Nichols, C. G., and Semenkovich, C. F. (2011) Fatty acid synthase modulates homeostatic responses to myocardial stress. *J. Biol. Chem.* **286**, 30949-30961
11. Abdalla, S., Fu, X., Elzahwy, S. S., Klaetschke, K., Streichert, T., and Quitterer, U. (2011) Up-regulation of the cardiac lipid metabolism at the onset of heart failure. *Cardiovasc. Hematol. Agents Med. Chem.* **9**, 190-206
12. Fu, X., Koller, S., Abd Alla, J., and Quitterer, U. (2013) Inhibition of G-protein-coupled receptor kinase 2 (GRK2) triggers the mitogen-activated protein kinase (MAPK) pathway. *J. Biol. Chem.* **288**, 7738-7755
13. Lucas, E., Jurado-Pueyo, M., Fortuno, M. A., Fernandez-Veledo, S., Vila-Bedmar, R., Jimenez-Borreguero, L. J., Lazcano, J. J., Gao, E., Gomez-Ambrosi, J., Frühbeck, G., Koch, W. J., Diez, J., Mayor, F., and Murga, C. (2014) Downregulation of G protein-coupled receptor kinase 2 levels enhances cardiac insulin sensitivity and switches on cardioprotective gene expression patterns. *Biochim. Biophys. Acta* **1842**, 2448-2456

14. Wang Y., Gao, E., Lau, W. B., Wang, Y., Liu, G., Li, J. J., Wang, X., Yuan, Y., Koch, W. J., and Ma, X. L. (2015) G-protein-coupled receptor kinase 2-mediated desensitization of adiponectin receptor in failing heart. *Circulation* **131**, 1392-1404
15. Chou I. P., Lin, Y. Y., Ding, S. T., and Chen, C. Y. (2014) Adiponectin receptor 1 enhances fatty acid metabolism and cell survival in palmitate-treated HepG2 cells through the PI3K/AKT pathway. *Eur. J. Nutr.* **53**, 907-917
16. Kim, J. E., Ahn, M. W., Baek, S. H., Lee, I. K., Kim, Y. W., Kim, J. Y., Dan, J. M., and Park, S. Y. (2008) AMPK activator, AICAR, inhibits palmitate-induced apoptosis in osteoblast. *Bone* **43**, 394-404
17. Quitterer, U., Pohl, A., Langer, A., Koller, S., and Abdalla, S. (2011) A cleavable signal peptide enhances cell surface delivery and heterodimerization of Cerulean-tagged angiotensin II AT1 and bradykinin B2 receptor. *Biochem. Biophys. Res. Commun.* **409**, 544-549
18. Abd Alla, J., El Faramawy, Y., and Quitterer, U. (2013) Microarray gene expression profiling reveals antioxidant-like effects of angiotensin II inhibition in atherosclerosis. *Front. Physiol.* **4**, 148
19. Abd Alla, J., Pohl, A., Reeck, K., Streichert, T., and Quitterer, U. (2010) Establishment of an in vivo model facilitates B2 receptor protein maturation and heterodimerization. *Integr. Biol.* **2**, 209-217
20. AbdAlla, S., Lother, H., el Missiry, A., Langer, A., Serveev, P., el Faramawy, Y., and Quitterer, U. (2009) Angiotensin II AT2 receptor oligomers mediate G-protein dysfunction in an animal model of Alzheimer disease. *J. Biol. Chem.* **264**, 6554-6565
21. Lorenz, K., Lohse, M. J., and Quitterer, U. (2003) Protein kinase C switches the Raf kinase inhibitor from Raf-1 to GRK2. *Nature* **426,** 574-579
22. Liu, L., Trent, C. M., Fang, X., Son, N. H., Jiang, H., Blaner, W. S., Hu, Y., Yin, Y. X., Farese, R. V., Homma, S., Turnbull, A. V., Eriksson, J. W., Hu, S. L., Ginsberg, H. N., Huang, L., S., and Goldberg, I. J. (2014) Cardiomyocyte-specific loss of diacylglycerol acyltransferase 1 (DGAT1) reproduces the abnormalities in lipids found in severe heart failure. *J. Biol. Chem.* **289**, 29881-29891
23. Kim, C., Wong, J., Wen, J., Wang, S., Wang, C., Spiering, S., Kan, N. G., Forcales, S., Puri, P. L., Leone, T. C., Marine, J. E., Calkins, H., Kelly, D. P., Judge, D. P., and Chen, H. S. (2013) Studying arrhythmogenic right ventricular dysplasia with patient-specific iPSCs. *Nature* **494**, 105-110
24. Biagi, P. L., Bordoni, A., Lorenzini, A., Horrobin, D. F., and Hrelia, S. (1999) Essential fatty acid metabolism in long term primary cultures of rat cardiomyocytes: a beneficial effect of n-6:n-3 fatty acids supplementation. *Mech. Ageing Dev.* **107**, 181-195
25. Lopaschuk, G. D., and Jaswal, J. S. (2010) Energy metabolic phenotype of the cardiomyocyte during development, differentiation, and postnatal maturation. *J. Cardiovasc. Pharmacol.* **56**, 130-140
26. Park, T. S., and Goldberg, I. J. (2012) Sphingolipids, lipotoxic cardiomyopathy, and cardiac failure. *Heart Fail. Clin.* **8**, 633-641
27. Mochly-Rosen, D., Das, K., and Grimes, K. V. (2012) Protein kinase C, an elusive therapeutic target? *Nat. Rev. Drug Discov.* **11**, 937-957
28. Liu, Q., and Molkentin, J. D. (2011) Protein kinase Cα as a heart failure therapeutic target. *J. Mol. Cell. Cardiol.* **51**, 474-478
29. Son, N.H., Yu, S., Tuinei, J., Arai, K., Hamai, H., Homma, S., Shulman, G. I., Abel, E. D., and Goldberg, I. J. (2010) PPARgamma-induced cardiolipotoxicity in mice is ameliorated by PPARalpha deficiency despite increases in fatty acid oxidation. *J. Clin. Invest.* **120**, 3443-3454
30. Graham, D. J., Ouellet-Hellstrom, R., MaCurdy, T. E., Ali, F., Sholley, C., Worrall, C., and Kelman, J. A. (2010) Risk of acute myocardial infarction, stroke, heart failure, and death in elderly medicare patients treated with rosiglitazone or pioglitazone. *JAMA* **304**, 411-418
31. Kliewer, S. A., Sundseth, S. S., Jones, S. A., Brown, P. J., Wisely, G. B., Koble, C. S., Devchand, P., Wahli, W., Willson, T. M., Lehnhard, J. M., and Lehmann, J. M. (1997) Fatty acids and eicosanoids regulate gene expression through direct interactions with peroxisome proliferator-activated receptors alpha and gamma. *Proc. Natl. Acad. Sci. USA* **94**, 4318-4323

32. Hamza, M. S., Pott, S., Vega, V. B., Thomsen, J. S., Kandhadayar, G. S., Ng, P. W., Chiu, K. P., Pettersson, S., Wei, C. L., Ruan, Y., and Liu, E. T. (2009) De-novo identification of PPARgamma/RXR binding sites and direct targets during adipogenesis. *PLoS One* **4**, e4907
33. Chirala, S. S., Chang, H., Matzuk, M., Abu-Elheiga, L. Mao, J., Mahon, K., Finegold, M., and Wakil, S. J. (2003) Fatty acid synthesis is essential in embryonic development: fatty acid synthase null mutants and most of the heterozygotes die in utero. *Proc. Natl. Acad. Sci. U.S.A.* **100**, 6358-6363
34. Knobloch, M., Braun, S. M., Zurkirchen, L., von Schoultz, C., Zamboni, N., Arauzo-Bravo, M. J., Kovacs, W. J., Karalay, O., Suter, U., Machado, R. A., Roccio, M., Lutolf, M. P., Semenkovich, C. F., and Jessberger, S. (2013) Metabolic control of adult neural stem cell activity by Fasn-dependent lipogenesis. *Nature* **493**, 226-230
35. Brinks, H., and Koch, W. J. (2010) Targeting G protein-coupled receptor kinases (GRKs) in heart failure. *Drug Discov. Today Dis. Mech.* **7**, e129-e134
36. Banks, A. S., McAllister, F. E., Camporez, J. P., Zushin, P. J., Jurczak, M. J., Laznik-Bogoslavski, D., Shulman, G. I., Gygi, S. P., and Spiegelman, B. M. (2015) An ERK/Cdk5 axis controls the diabetogenic actions of PPARG. *Nature* **517**, 391-395
37. Ungerer, M., Böhm, M., Elce, J. S., Erdmann, E., and Lohse, M. J. (1993) Altered expression of β-adrenergic receptor kinase and β1-adrenergic receptors in the failing human heart. *Circulation* **87**, 454-463
38. Piguet, A. C., Stroka, D., Zimmermann, A., and Dufour, J. F. (2009) Hypoxia aggravates non-alcoholic steatohepatitis in mice lacking hepatocellular PTEN. *Clin. Sci. (Lond.)* **118**, 401-410
39. Lee H. J., Ryu, J. M., Jung, Y. H., Oh, S. Y., Lee, S. J., and Han, H. J. (2015) Novel pathway for hypoxia-induced proliferation and migration in human mesenchymal stem cells: Involvement of HIF-1α, FASN and mTORC1. *Stem Cells* 33, 2182-2195
40. Choi, J. H., Banks, A. S., Estall, J. L., Kajimura, S., Bostrom, P., Laznik, D., Ruas, J. L., Chalmers, M. J., Kamenecka, T. M., Blüher, M., Griffin, P. R., and Spiegelman, B. M. (2010) Anti-diabetic drugs inhibit obesity-linked phosphorylation of PPARgamma by Cdk5. *Nature* **466**, 451-456
41. Zheng, H., Worral, C., Shen, H., Issad, T., Seregard, S., Girnita, A., and Girnita, L. (2012) Selective recruitment of G protein-coupled receptor kinases (GRKs) controls signaling of the insulin-like growth factor 1 receptor. *Proc. Natl. Acad. Sci. U.S.A.* **109**, 7055-7060
42. Lips, D. J., Bueno, O. F., Wilkins, B. J., Purcell, N. H., Kaiser, R. A., Lorenz, J. N., Voisin, L., Saba-El-Leil, M. K., Meloche, S., Poussegur, J., Pages, G., De Windt, L. J., Doevendans, P. A., and Molkentin, J. D. (2004) MEK-ERK2 signaling pathways protects myocardium from ischemic injury in vivo. *Circulation* **109**, 1938-1942
43. Hu, E., Kim, J. B., Sarraf, P., and Spiegelman, B. M. (1996) Inhibition of adipogenesis through MAP kinase-mediated phosphorylation of PPARgamma. *Science* **274**, 2100-2103
44. Dadson, K., Turdi, S., Hashemi, S., Zhao, J., Polidovitch, N., Beca, S., Backx, P. H., McDermott, J. C., and Sweeney, G. (2015) Adiponectin is required for cardiac MEF2 activation during pressure overload-induced hypertrophy. *J. Mol. Cell. Cardiol.* **86,** 102-109
45. Chemaly, E. R., Hadri, L., Zhang, S., Kim, M., Kohlbrenner, E., Sheng, J., Liang, L., Chen, J., K-Raman, P., Hajjar, R. J., and Lebeche, D. (2011) Long-term in vivo resistin overexpression induced myocardial dysfunction and remodeling in rats. *J. Mol. Cell. Cardiol.* **51**, 144-155
46. Liu, C., Feng, T., Zhu, N., Liu, P., Han, X., Chen, M., Wang, X., Li, N., Li, Y., Xu, Y., and Si, S. (2015) Identification of a novel selective agonist of PPARG with no promotion of adipogenesis and less inhibition of osteoblastogenesis. *Sci. Rep.* **5**, 9530
47. Murholm, M., Dixen, K., and Hansen, J. B. (2010) Ras signaling regulates differentiation and UCP1 expression in models of brown adipogenesis. *Biochim. Biophys. Acta* **1800**, 619-627
48. Joseph, J. W., Koshkin, V., Saleh, M. C., Sivitz, W. I., Zhang, C. Y., Lowell, B. B., Chan, C. B., and Wheeler, M. B. (2004) Free fatty acid-induced beta-cell defects are dependent on uncoupling protein 2 expression. *J. Biol. Chem.* **279**, 51049-51056

49. Li, N., Wang, J., Gao, F., Tian, Y., Song, R., and Zhu, S. J. (2010) The role of uncoupling protein 2 in the apoptosis induced by free fatty acid in rat cardiomyocytes. *J. Cardiovasc. Pharmacol.* **55**, 161-167
50. Bodyak, N., Rigor, D. L., Chen, Y. S., Han, Y., Bisping, E., Pu, W. T., and Kang, P. M. (2007) Uncoupling protein 2 modulates cell viability in adult rat cardiomyocytes. *Am. J. Physiol. Heart Circ. Physiol.* **293**, H829-H835 (2007).
51. George J., Patal, S., Wexler, D., Sharabi, Y., Peleg, E., Kamari, Y., Grossman, E., Sheps, D., Keren, G., and Roth, A. (2006) Circulating adiponectin concentrations in patients with congestive heart failure. *Heart* **92**, 1420-1424
52. O`Shea, K. M., Chess, D. J., Khairallah, R. J., Rastogi, S., Hecker, P. A., Sabbah, H. N., Walsh, K., and Stanley, W. C. (2010) Effects of adiponectin deficiency on structural and metabolic remodeling in mice subjected to pressure overload. *Am. J. Physiol. Heart Circ. Physiol.* **298**, H1639-H1645
53. Frankel, D. S., Vasan, R. S., D`Agostino, R. B., Benjamin, E. J., Levy, D., Wang, T. J., and Meigs, J. B. (2009) Resistin, adiponectin, and risk of heart failure the Framingham offspring study. *J. Am. Coll. Cardiol.* **53**, 754-762
54. Chatham, J. C., and Young, M. E. (2012) Metabolic remodeling in the hypertrophic heart: fuel for thought. *Circ. Res.* **111**, 666-668
55. Kujiraoka, T., Satoh, Y., Ayaori, M., Shiraishi, Y., Arai-Nakaya, Y., Hakuno, D., Yada, H., Kuwada, N., Endo, S., Isoda, K., and Adachi, T. (2013) Hepatic extracellular signal-regulated kinase 2 suppresses endoplasmic reticulum stress and protects from oxidative stress and endothelial dysfunction. *J. Am. Heart Assoc.* **2**, e000361
56. Marfella, R., Di Filippo, C., Portoghese, M., Barbieri, M., Ferraraccio, F., Siniscalchi, M., Cacciapuoti, F, Rossi, F., D`Amico, M., Paolisso, G. (2009) Myocardial lipid accumulation in patients with pressure-overloaded heart and metabolic syndrome. *J. Lipid Res*. **50**, 2314-2323
57. Hansmann, G., Wagner, R. A., Schellong, S, Perez, V. A., Urashima, T., Wang, L., Sheikh, A. Y., Suen, R. S., Stewart, D. J., and Rabinovitch, M. (2007) Pulmonary arterial hypertension is linked to insulin resistance and reversed by peroxisome proliferator-activated receptor-gamma activation. *Circulation* **115**, 1275-1284
58. Woodall, M. C., Ciccarelli, M., Woodall, B. P., and Koch, W. J. (2014) G protein-coupled receptor kinase 2: a link between myocardial contractile function and cardiac metabolism. *Circ. Res.* **114**, 1661-1670
59. Dy, G. K., and Adjei, A. A. (2013) Understanding, recognizing, and managing toxicities of targeted anticancer therapies. *CA Cancer J. Clin.* **63**, 249-279


**FOOTNOTES**

This work was supported in part by the Swiss National Science Foundation (grant number 31-140679 to U.Q.).

The abbreviations used are: AAC, abdominal aortic constriction; *Acaca*, acetyl-CoA carboxylase alpha; *Adipoq*, adiponectin; *Adipor1*, adiponectin receptor protein 1; *Arrb1*, beta-arrestin-1; B6 mice, C57BL/6J mice; BrdU, 5-bromo-2`-deoxyuridine; CPT-1, carnitine palmitoyl transferase 1; DAG, diacylglycerol; 2-DG, 2-deoxyglucose; ECAR, extracellular acidification rate; ERK, extracellular signal-regulated kinase; FASN, fatty acid synthase; FFA, free fatty acids; GO, gene ontology; GRK2, G-protein-coupled receptor kinase-2; GRKInh, GRK2-specific peptide inhibitor with the peptide sequence MAKFERLQTVTNYFITSE; IBMX, 3-isobutylmethylxanthine; MAPK, mitogen-activated protein kinase; α-MHC, α-myosin heavy chain; MEM, minimum essential medium; OCR, oxygen consumption rate; *PPARG*, peroxisome proliferator-activated receptor γ; *Prkaa1/2*, protein kinase, AMP-activated alpha 1/2 catalytic subunit; *Retn*, resistin; RKIP, raf kinase inhibitor protein; Tg-*FASN* mice, transgenic mice with myocardium-specific expression of *FASN*; TUNEL, terminal deoxynucleotidyl transferase-mediated dUTP nick-end labelling; *UCP1*, uncoupling protein 1.

## FIGURE LEGENDS

**Figure 1.** *FASN*-transgenic cardiomyocytes developed a dysfunctional cardiac substrate metabolism. *A*, Scheme of the α-MHC-*FASN* vector used for the generation of *FASN*-transgenic mice. *B*, Identification of the α-MHC-*FASN* transgene in the genomic DNA of different founder mice by PCR. The asterisks denote the amount of the *FASN* transgene-specific PCR product [***,**,*: >, =, < amount of PCR product obtained with 2 ng of plasmid template (P)]. *C*, Immunoblot detection of the FASN protein in hearts from different founder mice with FASN-specific antibodies (IB: FASN). The asterisks indicate the amount of transgenic FASN protein relative to the non-transgenic control after normalization to Gnb [***, 2.5-fold; **, 2.3-fold; *, 1.8-fold (no. 5) and 1.4-fold (no. 10) increase over control]. The lower panel shows a control immunoblot detecting Gnb. *D*, *E*, Real-time measurement of the oxygen consumption rates (OCR) and extracellular acidification rates (ECAR) of neonatal cardiomyocytes isolated from *FASN*-transgenic (Tg-*FASN*) and B6 control mice under basal conditions (left) and after the creation of an adult-like lipogenic milieu by the 3F protocol for 10 days (right). The addition of the CPT-1 inhibitor, Etomoxir (Etom., 50 μM) and 2-deoxyglucose (2-DG, 50 mM) is indicated by the arrows. The relative values normalised to the baseline (i.e., the second measurement point set to 100%) (*D*), and the absolute values of OCR and ECAR (*E*) are presented. *F*, *G*, The Etomoxir-blocked fraction of the OCR represents fatty acid β-oxidation, the 2-deoxyglucose-blocked fraction of the ECAR represents glycolysis, and the ratio of glycolysis/β-oxidation was calculated. The data are shown as the means ± s.d.; n=6 technical replicates (*D*, *E*), and n=3 biological replicates (*F*, *G*); ***,$P$=0.0002 (*F*, left) and 0.0004 (*G*, right); **,$P$=0.0032 (*F*, middle), 0.0079 (*F*, right) and 0.0071 (*G*, left); $P$=0.7324 (*G*, middle).

**Figure 2.** *FASN*-transgenic mice developed signs of heart failure and cardiac lipid load. *A*, Decreased left ventricular ejection fraction of 6 month-old Tg-*FASN* mice. *B*, Histological analysis of a Tg-*FASN* heart compared to a B6 heart (bar: 2 mm). *C*, Increased heart-weight-to-body-weight ratio of Tg-*FASN* mice. *D*, *E*, Increased number of TUNEL-positive cardiomyocytes of Tg-*FASN* hearts. Panel (*E*) shows representative immunohistological sections (bar: 20 μm). The data shown are the mean ±s.d., n=5; ***,$P$<0.0001 (*A*, *C*, *D*). *F*-*H*, Detection of the cardiac FASN protein levels by immunoblotting (*F,G*) and immunohistology (*H*) relative to the B6 control (bar: 40 μm). Panel (*F*) shows quantitative data that were obtained by densitometric scanning of immunoblots (± s.d., n=4; ***,$P$=0.0005). *I*-*L*, The cardiac free fatty acid, FFA (*I*), triacylglycerol, TAG (*J*), diacylglycerol, DAG (*K*), and total ceramide (*L*) contents of Tg-*FASN* mice relative to non-transgenic B6 controls [±s.d., n=5; ***,$P$=0.0006 (*I*), 0.0004 (*J*) and 0.0001 (*K*); **,$P$= 0.0028]. Histology experiments are representative of four different mice/group (*B*, *H*).

**Figure 3.** Up-regulation of the heart failure-related cardiac lipid metabolic process in *FASN*-transgenic mice. *A*, Microarray gene expression profiling identified significantly up-regulated heart failure-related genes of the lipid metabolic process in hearts of 6 month-old Tg-*FASN* mice compared to B6 mice. *B*, The heart failure-related adipogenic gene signature was similarly detected in 10 month-old B6 mice with heart failure induced by six months of AAC compared to age-matched sham controls (Sham-6mo). *C*, Adipogenic genes were not significantly up-regulated in 5 month-old B6 mice with cardiac hypertrophy induced by 1 month of ACC (Cardiac hypertrophy) in the absence of heart failure signs compared to the sham control (Sham-1mo). *D*, Significantly up-regulated genes of the lipid metabolic process in hearts of 8 month-old ApoE$^{-/-}$ mice with 2 months of *Pparg* activation with rosiglitazone compared to untreated ApoE$^{-/-}$ mice. The probe sets were categorised into genes involved in lipid synthesis, storage, oxidation, and adipocyte differentiation. The statistical significance of the microarray data was evaluated using signal intensity values of probe sets (*,$P$<0.05; **,$P$≤0.01; ***,$P$≤0.001 vs. the respective control; ±s.d., n=2 gene chips per group, cRNA pooled from 4 mice/gene chip).

**Figure 4.** Down regulation of endogenous *Fasn* reveals a causal relationship between *Fasn* and *Pparg* activation in promoting cardiac dysfunction. *A*, *B*, Stable integration of lentiviral mi*Fasn*-DNA into the genomic DNA of ApoE-/- mouse hearts (H1, H2), kidneys (K1, K2) and livers (L1, L2) isolated two

months after lentiviral transduction. Control DNA (cont. DNA) was isolated from an ApoE-/- mouse. In (*B*), the genomic integration of lentiviral DNA was quantified by qPCR (±s.d.; n=6; ***,*P*<0.001; *,*P*<0.05 vs. Heart). *C*, Lentivirus-mediated delivery of mi*Fasn* decreased the expression of *Fasn* in hearts of ApoE-/- mice with 2 months of *Pparg* activation by rosiglitazone (±s.d.; n=3; **,*P*=0.0029). *D*, *E*, Immunohistological detection of Fasn (*D*) with anti-Fasn antibodies (anti-Fasn), and total lipids by oil red O staining (*E*) in cardiac sections of ApoE-/- mice after 2 months of *Pparg* activation and transduction of a control lentivirus (miCon) or lentiviral delivery of mi*Fasn* (bar: 40 μm). *F*, Lentivirus-mediated delivery of mi*Fasn* normalised the enhanced cardiomyocyte apoptosis of ApoE-/- mice that was triggered by *Pparg* activation (±s.d.; n=3; **,*P*=0.0031). The right panels show representative immunohistology images of TUNEL staining (bar: 20 μm). *G*, Viral transduction of ApoE-/- mice with a lentivirus that targets *Fasn* by RNAi (mi*Fasn*) retarded the increase in the heart-weight-to-body-weight ratio that was induced by two months of *Pparg* activation with rosiglitazone (±s.d.; n=6; **,*P*=0.0011). *H*, Histological analysis of hearts from 8 month-old ApoE-/- mice isolated after two months of *Pparg* activation and transduction of a control lentivirus (miCon) or mi*Fasn* (bar: 2 mm). *I*, Left ventricular ejection fraction of ApoE-/- mice after two months of *Pparg* activation and transduction of a control lentivirus (miCon) or mi*Fasn* (±s.d.; n=6; ***,*P*=0.0002). Histology experiments are representative of four different mice/group (*D*, *E*, *H*).

**Figure 5.** GRK2 inhibition by GRKInh in *FASN*-transgenic mice. *A*, Cardiac up-regulation of the GRK2 protein level in Tg-*FASN* relative to B6 hearts was detected by immunoblotting with GRK2-specific antibodies (n=4 mice/group). The lower panel is a control immunoblot detecting Gnb. The right panel shows the quantitative immunoblot evaluation (±s.d., n=4). *B*, Immunoaffinity enrichment of GRKInh (AP, +) with GRKInh-specific antibodies from Tg-GRKInh/*FASN* hearts, and immunoblot detection (IB) of co-enriched GRK2 protein (left panel) and GRK5 protein (right panel). The control experiment (AP, -) applied an affinity matrix with immobilised control IgG. The lower panels show immunoblot detection of enriched GRKInh. *C*, Quantitative assessment of the GRKInh-GRK-interaction. GRK2 and GRK5 protein levels were determined by immunoblotting with GRK2-specific and GRK5-specific antibodies, respectively, of cardiac lysates from Tg-GRKInh/*FASN* mice before (total) and after (not bound to GRKInh) incubation with an affinity matrix with immobilised anti-GRKInh antibodies. The left and middle panels present data evaluation from 3 independent experiments (±s.d., n=3), and the right panels show representative immunoblots. *D*, Immunofluorescence co-localization of Arrb1 with p38 MAPK in cardiac sections from Tg-*FASN* and Tg-GRKInh/*FASN* mice (bar: 20 μm). Arrb1 was detected with affinity-purified mouse anti-Arrb1 antibodies followed by $F(ab)_2$ fragments of Alexa Fluor 546-labelled (red) secondary antibodies, and p38 was detected with affinity-purified rabbit anti-p38 MAPK antibodies followed by $F(ab)_2$ fragments of Alexa Fluor 488-labelled (green) secondary antibodies. Cell nuclei were stained with DAPI (blue). Immunofluorescence experiments are representative of four different mice/group.

**Figure 6.** GRK2 inhibition by GRKInh prevents the dysfunctional cardiac energetics of *FASN*-transgenic cardiomyocytes. *A*, *B*, The development of a dysfunctional cardiomyocyte energetics of *FASN*-transgenic cardiomyocytes was retarded in double-transgenic mice that co-expressed the GRK2-inhibitor, GRKInh. Real-time measurements of OCR and ECAR of neonatal cardiomyocytes isolated from *FASN*-transgenic (Tg-*FASN*), double-transgenic Tg-GRKInh/*FASN* and non-transgenic B6 mice were performed under basal conditions (left panels) and after treatment with the 3F protocol (right panels). The OCR and ECAR values normalised to the baseline (*A*), and the absolute values of OCR and ECAR (*B*) are presented. *C*-*E*, The Etomoxir-blocked fraction of OCR, which represents fatty acid β-oxidation (*C*), the 2-deoxyglucose-blocked fraction of ECAR, which represents glycolysis (*D*), and the ratio of glycolysis/β-oxidation (*E*) were determined with cardiomyocytes isolated from Tg-*FASN*, Tg-GRKInh/*FASN*, B6 and Tg-GRKInh mice. The data are shown as the means ± s.d.; n=6 technical replicates (*A*, *B*) and n=3 biological replicates (*C*-*E*); *,*P*<0.05, **,*P*<0.01 and ***,*P*<0.001 vs. Tg-*FASN*. *F*, Cardiomyocytes from Tg-GRKInh/*FASN* (lanes 3,4) mice showed significant adiponectin (Adipoq)- stimulated activation of Prkaa relative to Tg-*FASN* cardiomyocytes (lanes 1,2). Cardiomyocytes (3F protocol) were stimulated without

(-) and with (+) globular domain adiponectin (2 μg/ml) for 60 min, and the activation of Prkaa was determined by immunoblotting with phospho-Prkaa- (p-Prkaa)-specific antibodies. The left panel presents quantitative data from 4 independent experiments (±s.d.; n=4; ***,$P$<0.0001), and the middle and right panels show representative immunoblots.

**Figure 7.** GRKInh retards the development of heart failure signs in Tg-*FASN* mice and promotes ERK axis-dependent inhibition of *Pparg* transcriptional activity. *A*, *B*, Cardiac free fatty acid, FFA (*A*), and triacylglycerol, TAG (*B*), contents of Tg-*FASN* mice relative to double-transgenic Tg-GRKInh/*FASN*, non-transgenic B6, and single-transgenic Tg-GRKInh mice (±s.d., n=5; *,$P$<0.05 vs. Tg-*FASN* and Tg-GRKInh; **,$P$<0.01 vs. Tg-*FASN*; ***,$P$<0.001 vs. Tg-*FASN*). *C*, Cardiac *Acaca* expression in Tg-*FASN*, double-transgenic Tg-GRKInh/*FASN*, B6 and Tg-GRKInh mice (±s.d. n=5; ***,$P$<0.001 vs. Tg-GRKInh/*FASN*, B6 and Tg-GRKInh hearts). *D*, Cardiac expression of transgenic *FASN* (left panel) (± s.d., n=5; ***, $P$<0.001 vs. B6), and expression of the endogenously expressed murine *Fasn* (right panel) (±s.d.; n=5; ***, $P$<0.001 vs. Tg-GRKInh/*FASN* and B6). *E*, Immunoblot detection of the FASN/Fasn protein in cardiac tissue extracts from Tg-*FASN* relative to Tg-GRKInh/*FASN* mice (±s.d.; n=5 hearts/group; **,$P$=0.0016). *F-H*, The left ventricular ejection fraction (*F*), the heart-weight-to-body-weight ratio (*G*), and the cardiac ATP content (*H*) of Tg-*FASN* mice relative to double-transgenic Tg-GRKInh/*FASN* mice and age-matched B6 controls (± s.d., n=5; *,$P$<0.05, **,$P$<0.01 and ***$P$<0.001 vs. Tg-*FASN*). *I*, The number of TUNEL-positive cardiomyocytes (± s.d., n=5; ***$P$<0.001 vs. Tg-*FASN*). The right panel shows representative immunohistological sections of TUNEL staining (bar: 20 μm). *J*, Immunohistological detection of activated phospho-ERK1/2 in cardiac sections of a Tg-*FASN* mouse relative to a Tg-GRKInh/*FASN* mouse (bar: 40 μm). Histology experiments are representative of four different mice/group. *K*, Immunoblot detection of activated phospho-ERK1/2 (upper) and total ERK1/2 (lower) in cardiac tissue extracts from Tg-*FASN* relative to Tg-GRKInh/*FASN* mice (n=4 hearts/group). *L*, Immunoblot detection of pS273-Pparg (upper) and total Pparg (lower) in cardiac tissue extracts from Tg-*FASN* and Tg-GRKInh/*FASN* mice (n=4 hearts/group). *M*, *N*, Immunoblot detection (*M*) of pS273-Pparg (upper panel), pS112-Pparg (middle panel), and Pparg (lower panel), respectively, and *Pparg* activity of nuclear extracts (*N*) from Tg-*FASN* relative to Tg-GRKInh/*FASN* cardiomyocytes (3F protocol) treated without (-) or with (+) the MEK inhibitor PD0325901 (0.5 μM) (±s.d.; n=4; ***,$P$<0.001). *O*, Cardiac expression of heart failure-related *Pparg* target genes in Tg-*FASN*, double-transgenic Tg-GRKInh/*FASN*, and B6 control mice (±s.d.; n=4; ***,$P$<0.001 vs. Tg-GRKInh/*FASN* and B6).

**Figure 8.** Inhibition of *Fasn* decreases cardiolipotoxicity induced by serine-273 phosphorylation-deficient *PPARG-S273A*. *A*, *B*, Neonatal rat cardiomyocytes were transfected with *PPARG* or *PPARG-S273A* mutant, and incubated in the absence (-) or presence (+) of rosiglitazone (Rosiglit., 5 μM), and *Fasn* was inhibited by RNAi (si*Fasn*) as indicated. The free fatty acid (*A*) and ATP (*B*) contents of cardiomyocytes were determined [±s.d.; n=4; *,$P$<0.05; **, $P$<0.01; ***,$P$<0.001 vs. controls transfected with stealth control RNAi (-); Dunnett`s multiple comparison test]. *C*, Immunoblot detection of Fasn (upper panel) and PPARG (middle panel) in cardiomyocyte lysates. The lower panel is a control immunoblot detecting Gnb. *D*, Immunofluorescence localization of Fasn (red) and the transmembrane-spanning AT1 receptor (AT1R; green) in cardiomyocytes without (Control) or with transfection of *PPARG*, *PPARG-S273A*, si*Fasn* and treatment with rosiglitazone (Rosiglit.) as indicated. Fasn was detected with affinity-purified rabbit anti-Fasn antibodies followed by $F(ab)_2$ fragments of Alexa Fluor 546-labelled secondary antibodies, and AT1R was detected with affinity-purified rat anti-AT1R antibodies followed by $F(ab)_2$ fragments of Alexa Fluor 488-labelled secondary antibodies. Cell nuclei were stained with DAPI (blue; bar: 20 μm). The immunofluorescence data are representative of four independent experiments.

**Figure 9.** GRK2 inhibition retards up-regulation of heart failure-related *Ucp1* and mitochondrial uncoupling. *A*, Immunoblot detection of Ucp1 protein in heart tissue extracts of Tg-*FASN* relative to Tg-GRKInh/*FASN* mice (n=4 hearts/group). The lower panel shows a control immunoblot detecting Gnb. *B*, Increased oligomycin-insensitive OCR of Tg-*FASN* cardiomyocytes relative to Tg-GRKInh/*FASN*

cardiomyocytes (3F) treated for 72 h without (-) or with (+) the MEK inhibitor PD0325901 [±s.d.; n=4; *,$P$<0.05 vs. TgGRKInh/*FASN*(-); **,$P$<0.01 vs. Tg*FASN*]. Baseline OCR (3F) of Tg-*FASN*, Tg-GRKInh/*FASN* and Tg-GRKInh/*FASN* (+PD) was 13.68±0.98, 22.73±2.18 and 18.09±2.62 pmol/min per μg protein, respectively (±s.d.; n=4). *C*, Immunoblot detection of Ucp1 protein of Tg-*FASN* cardiomyocytes relative to Tg-GRKInh/*FASN* cardiomyocytes treated for 72 h without (-) or with (+) PD0325901 [±s.d.; n=4; *,$P$<0.05 vs. Tg-GRKInh/*FASN* (-); ***,$P$<0.001 vs. Tg-*FASN*]. The right panels show a representative immunoblot experiment.

**Figure 10.** Transgenic Tg-*UCP1* mice developed signs of heart failure and mitochondrial uncoupling. *A*, The transgenic vector used for the generation of Tg-*UCP1* mice with myocardium-specific *UCP1* expression. *B*, PCR identification of founder mice with stable integration of the *UCP1* transgene into the genomic DNA. *C*, *D*, Immunoblots show the detection of UCP1 protein in 6 month-old Tg-*UCP1* hearts (Tg-6) relative to age-matched B6 hearts (*C*), and Tg-11 hearts (*D*), respectively (n=4 hearts/group; the last lane of panel (*D*) is an additional B6 control). The lower panels show control immunoblots detecting Gnb. *E*, *F*, Left ventricular ejection fraction (*E*) and cardiac ATP content (*F*) of 6 month-old Tg-*UCP1* mice (Tg-6) relative to Tg-11 mice and B6 controls (±s.d.; n=5; ***,$P$<0.001 vs. B6 control; Dunnett`s multiple comparison test). *G*, Heart-weight-to-body-weight ratio of Tg-*UCP1* relative to B6 mice (±s.d.; n=5). *H*, Representative histological section of a 6 month-old Tg-*UCP1* heart relative to an age-matched B6 control (bar: 2 mm). Histology experiments are representative of four different mice/group. *I*, Immunoblot detection of Fasn protein in cardiac tissue extracts from Tg-*UCP1* relative to B6 mice (±s.d.; n=4). The left panel shows a representative immunoblot detection for Fasn. *J*, Increased oligomycin-insensitive OCR of Tg-*UCP1* cardiomyocytes relative to B6 cardiomyocytes (±s.d.; n=4 biological replicates; 3F protocol). The right panel shows baseline OCR values. *K*, FFA (left panel) and ATP contents (middle panel) of isolated neonatal cardiomyocytes from B6 mice after transfection without (-) or with (+) *PPARG*, *PPARG-S273A*, si*Ucp1* and treatment with rosiglitazone (+rosiglit.) as indicated [±s.d.; n=4; *,$P$<0.05; **, $P$<0.01; ***,$P$<0.001 vs. control transfected with stealth control RNAi (-); Dunnett`s multiple comparison test]. The right panels show immunoblot detection of Ucp1 and PPARG.

**Figure 11.** Cardioprotective GRK2 inhibition requires an intact ERK axis. *A*, Isoproterenol-stimulated (100 nM) cAMP levels of neonatal cardiomyocytes isolated from RKIP-transgenic, GRKInh-transgenic and B6 mice (±s.d., n=3; ***,$P$<0.001 vs. B6). *B*, Immunoblot detection of pS273-Pparg (upper) and total Pparg (lower) in cardiac tissue extracts of RKIP-transgenic mice relative to B6 controls. *C*, Quantitative evaluation of immunoblot data (±s.d., n=3; ***,$P$<0.001 and **,$P$<0.01 vs. RKIP; and *,$P$<0.05 vs. B6). *D*, Gene expression data showed up-regulation of the cardiac *Pparg*-dependent lipid metabolic process of 6 month-old Tg-RKIP mice compared to B6 controls (***,$P$<0.001, **,$P$<0.01, *,$P$<0.05 vs. B6). *E*, *F*, Cardiac FFA (*E*) and triacylglycerol, TAG (*F*) contents of RKIP-transgenic relative to B6 control hearts (±s.d., n=5; ***,$P$=0.0006). *G*, Oil red O detection of cardiac lipids in a cardiac section from an RKIP-transgenic vs. a B6 control heart (bar: 40 μm). Histology experiments are representative of four different mice/group. *H*, Decreased left ventricular ejection fraction of RKIP-transgenic mice indicates cardiac dysfunction (±s.d., n=5; ***,$P$<0.0001). *I*, *J*, Real-time measurement of OCR (*I*) and ECAR (*J*) of neonatal cardiomyocytes from RKIP-transgenic mice was performed under basal conditions and after the creation of an adult-like lipogenic milieu by the 3F protocol. Neonatal cardiomyocytes from Tg-GRKInh mice were measured under basal conditions. The relative values normalised to the baseline (upper panels), and the absolute values of OCR and ECAR (lower panels) are presented. *K-M*, The Etomoxir-blocked fraction of OCR, which represents fatty acid β-oxidation (*K*), the 2-deoxyglucose-blocked fraction of ECAR, which represents glycolysis (*L*), and the ratio of glycolysis/β-oxidation (*M*) are also given. The data are shown as the means ± s.d.; n=6 technical replicates (*I*, *J*) and n=3 biological replicates (*K-M*); ***,$P$<0.001 vs. RKIP (*K*, *M*), **,$P$<0.01 vs. RKIP-3F (*L*) and RKIP (*M*) and *,$P$<0.05 vs. RKIP-3F (*L*, *M*).

**Figure 12.** GRK2 inhibition retards the development of heart failure signs, cardiac lipid load and *Pparg* target gene induction in a pressure overload-induced heart failure model. *A*, Representative histological

sections of hearts from a 10-month-old B6 mouse (AAC) relative to an age-matched GRKInh-transgenic mouse (AAC+GRKInh) after 6 months of pressure overload imposed by AAC. The lower panels show age-matched sham-operated control hearts, bar: 2 mm. *B*, *C*, The heart-weight-to-body-weight ratio (*B*), and the left ventricular ejection fraction (*C*) of 10-month-old GRKInh-transgenic mice with 6 months of AAC (AAC+GRKInh) relative to age-matched non-transgenic B6 mice with 6 months of AAC (AAC). Age-matched sham-operated non-transgenic B6 mice (Sham) and sham-operated GRKInh-transgenic mice (Sham+GRKInh) served as controls. Data are shown as the means ± s.d., n=4 (*,$P$<0.05 vs. AAC+GRKInh; **,$P$<0.01 vs. AAC; ***,$P$<0.001 vs. AAC). *D*, Immunoblot detection of Fasn in cardiac tissue extracts of 10-month-old B6 mice with 6 months of AAC relative to age-matched GRKInh-transgenic mice with 6 months of AAC (n=4 hearts/group, left blot). Under the experimental conditions, the Fasn protein (lane 1, A, positive control of a 10-month-old B6 heart with 6 months of AAC) was not detectable in cardiac tissue extracts from sham-operated B6 (sham) or GRKInh-transgenic mice (n=2; right blot). The lower panels show control immunoblots detecting Gnb. *E*, Oil red O staining of cardiac sections from the different groups of mice (bar: 40 μm). Histology experiments are representative of four different mice/group (*A*, *E*). *F*, *G*, The number of TUNEL-positive cardiomyocytes (±s.d.; n=4; ***,$P$<0.001 vs. AAC). Panel (*F*) shows representative immunohistological sections of TUNEL staining (bar: 20 μm). *H*, *I*, Immunoblot detection of pS273-Pparg (upper panels) and total Pparg (lower panels) in cardiac tissue extracts from the different groups of mice [n=4 hearts/group (*H*), and n=2 hearts/group (*I*)]. *J*, Expression of heart failure-related *Pparg* targets in hearts from 10-month-old B6 mice with 6 months of AAC (AAC) and age-matched Tg-GRKInh mice with 6 months of AAC (AAC+GRKInh) relative to sham-operated controls (±s.d.; n=4; ***,$P$<0.001 vs. AAC+GRKInh, Sham, and Sham+GRKInh).

**Figure 13.** Down-regulation of endogenous *Ucp1* retards the development of cardiac dysfunction in a pressure overload-induced heart failure model. *A*, *B*, Endogenous *Ucp1* expression (*A*) and Ucp1 protein level (*B*) in hearts of B6 mice with 2 months of AAC and transduction of a control lentivirus (AAC+miCont.) or a lentivirus targeting *Ucp1* by RNAi (AAC+mi*Ucp1*) relative to sham-operated B6 controls. (*C*) Down-regulation of *Ucp1* retarded the AAC-triggered decrease in the left ventricular ejection fraction (AAC+mi*UCP1*) relative to AAC-subjected B6 mice transduced with a control lentivirus (AAC+miCont.). The data are shown as the means ± s.d. (n=4; *,$P$<0.05 and ***,$P$<0.001 vs. Sham B6; Dunnett`s multiple comparison test).

**Figure 14.** Low efficacy of GRKInh in retarding the cardiac phenotype of *PPARG*-S273A-transgenic mice. *A*, A transgenic vector used for the generation of transgenic mice with myocardium-specific expression of *PPARG* (and *PPARG*-S273A). *B*, Cardiac sections from newborn transgenic mice that expressed *PPARG*-S273A or wild-type *PPARG* relative to a non-transgenic B6 control. Histological sections were stained with hematoxylin-eosin (H&E), and are representative of three mice/groups. *C*, Immunoblot detection of PPARG/Pparg in cardiac tissue extracts of 4-week-old mice with transgenic *PPARG*-S273A (S273A) expression or *PPARG* expression (as indicated) relative to non-transgenic B6 controls (n=4 hearts/group). The lower panel is a control immunoblot detecting Gnb. *D*, *E*, The cardiac expression of *PPARG* (*D*), and the heart-weight-to-body-weight ratio (*E*) of 4-week-old transgenic mice with expression of *PPARG*-S273A (S273A), *PPARG*-S273A+GRKInh, *PPARG* and *PPARG*+GRKInh are shown relative to age-matched non-transgenic B6 mice (±s.d., n=4; *,$P$<0.05; ***,$P$<0.001 vs. B6 control, Dunnett`s multiple comparison test). *F*, Increased postnatal mortality of mice with myocardium-specific expression of *PPARG*-273A and *PPARG*-S273+GRKInh compared to mice expressing *PPARG* and *PPARG*+GRKInh, respectively. *G*, Gene expression analysis of heart failure-related *Pparg* targets in hearts from 4-week-old transgenic mice that express *PPARG*-S273, *PPARG*-S273+GRKInh, *PPARG*, *PPARG*+GRKInh relative to non-transgenic B6 hearts (±s.d., n=4, *,$P$<0.05 and ***,$P$<0.001 vs. B6 control, Dunnett`s multiple comparison test). *H*, The cardiomyocyte energetics was determined with neonatal cardiomyocytes isolated from transgenic mice with myocardium-specific expression of *PPARG*-S273A (S273A), *PPARG*-S273A+GRKInh, *PPARG*, *PPARG*+GRKInh and non-transgenic B6 mice. The Etomoxir-blocked fraction of OCR, which represents fatty acid β-oxidation (left panels), the 2-deoxyglucose-blocked fraction of ECAR, which represents glycolysis (middle panels), and the ratio of

glycolysis/β-oxidation (right panels) were determined under basal conditions (upper panels) and after the creation of an adult-like lipogenic milieu by the 3F protocol for 10 days (lower panels). The data are shown as the means ± s.d.; n=3 biological replicates; *,$P<0.05$, **,$P<0.01$ and ***$P<0.001$ vs. B6; Dunnett`s multiple comparison test).

**Figure 15.** The scheme illustrates cardioprotective effects of GRK2 inhibition, which target the cardiometabolic dysfunction of late-stage heart failure. The histology image presents a cardiac section from an 8 month-old ApoE-/- mouse with signs of heart failure induced by 2 months of *Pparg* activation with rosiglitazone.

**Figure 1**

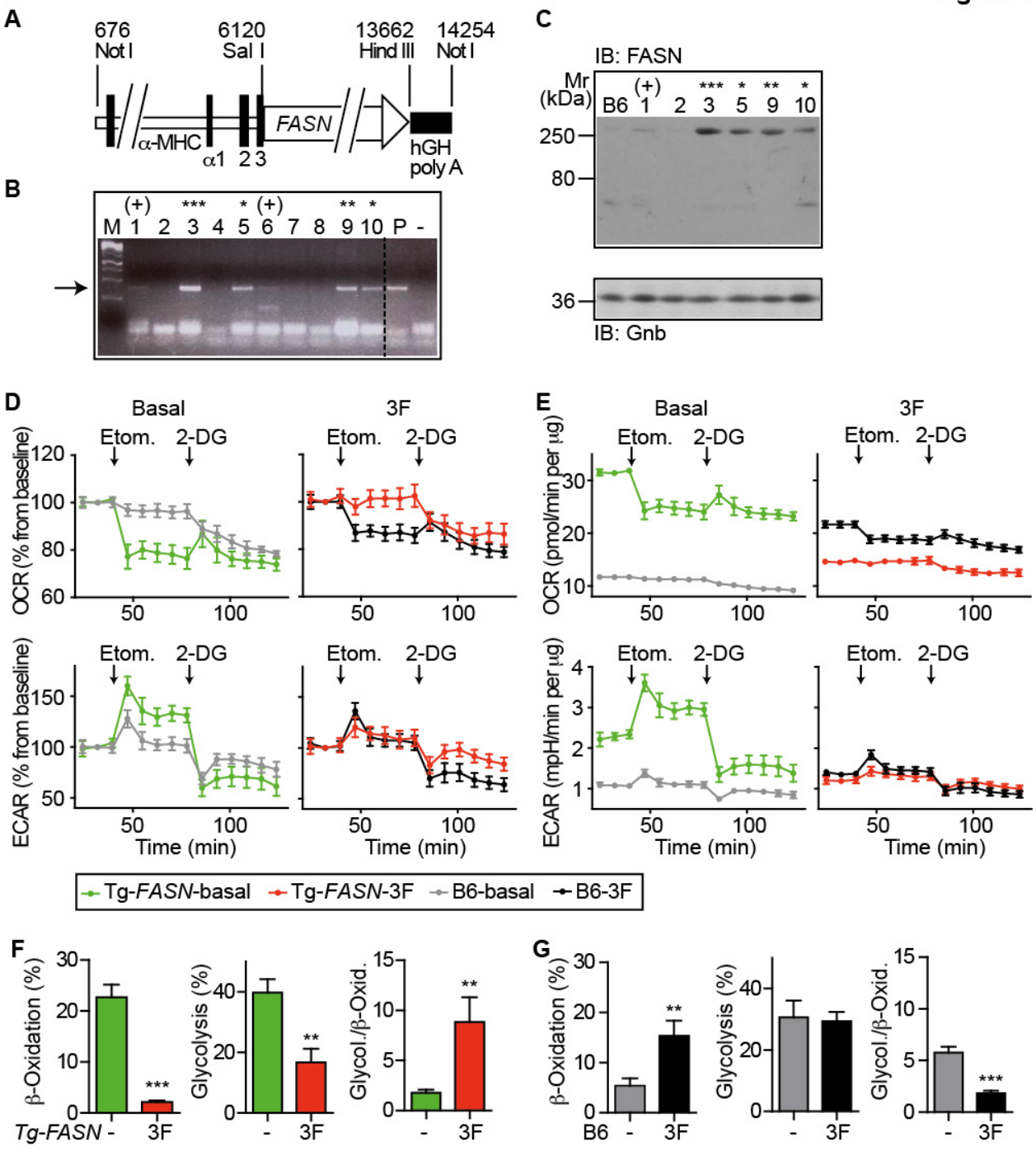

**Figure 2**

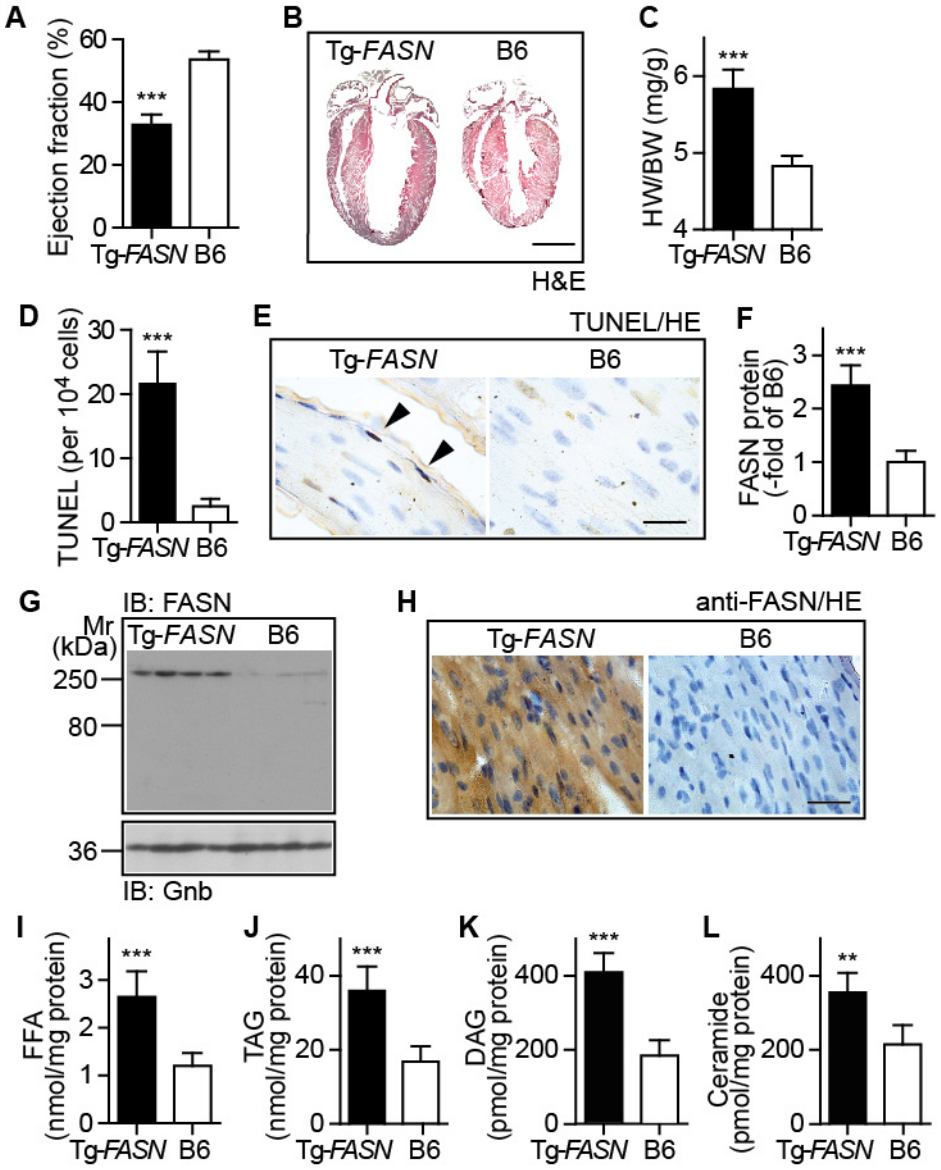

**Figure 3**

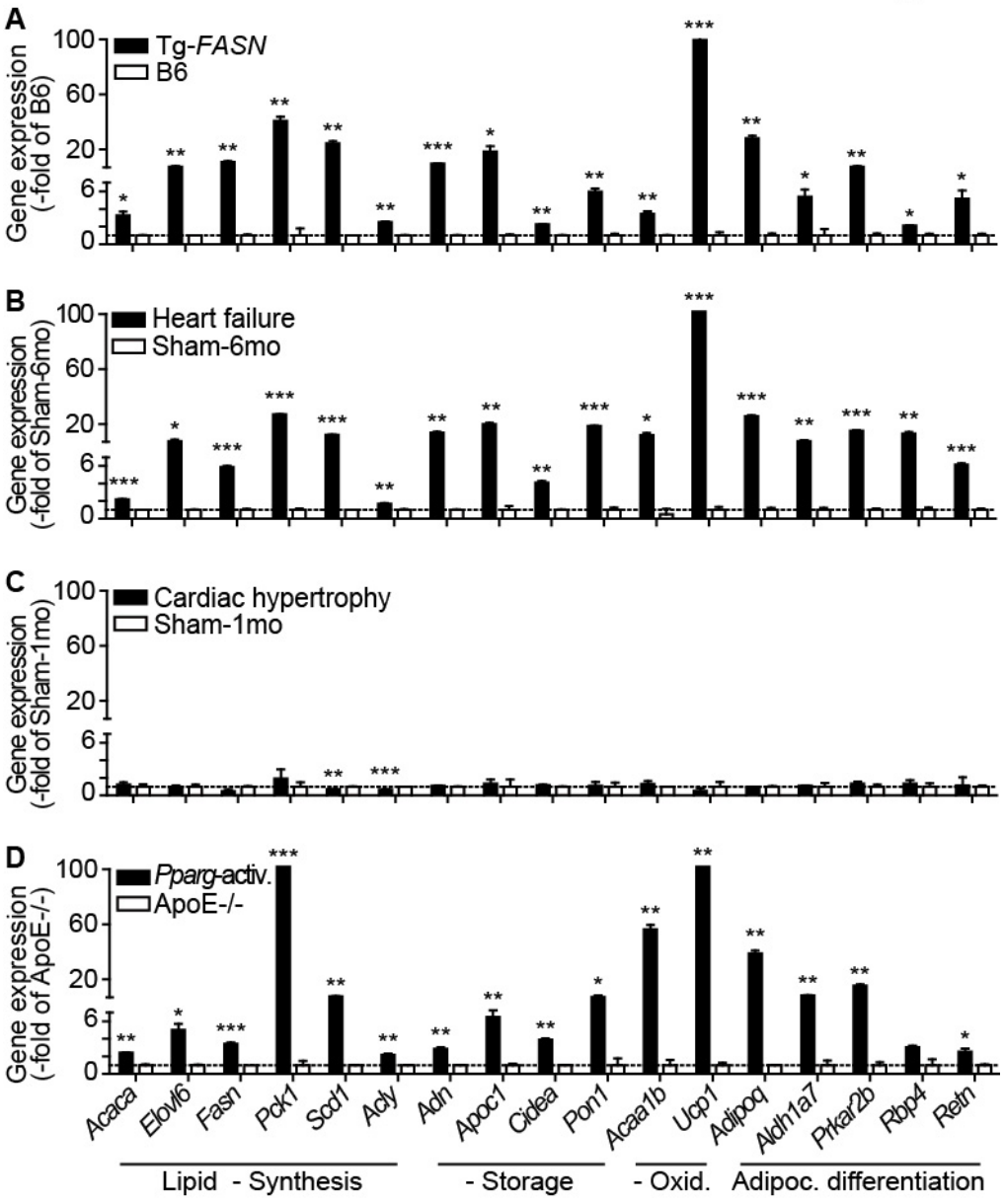

**Figure 4**

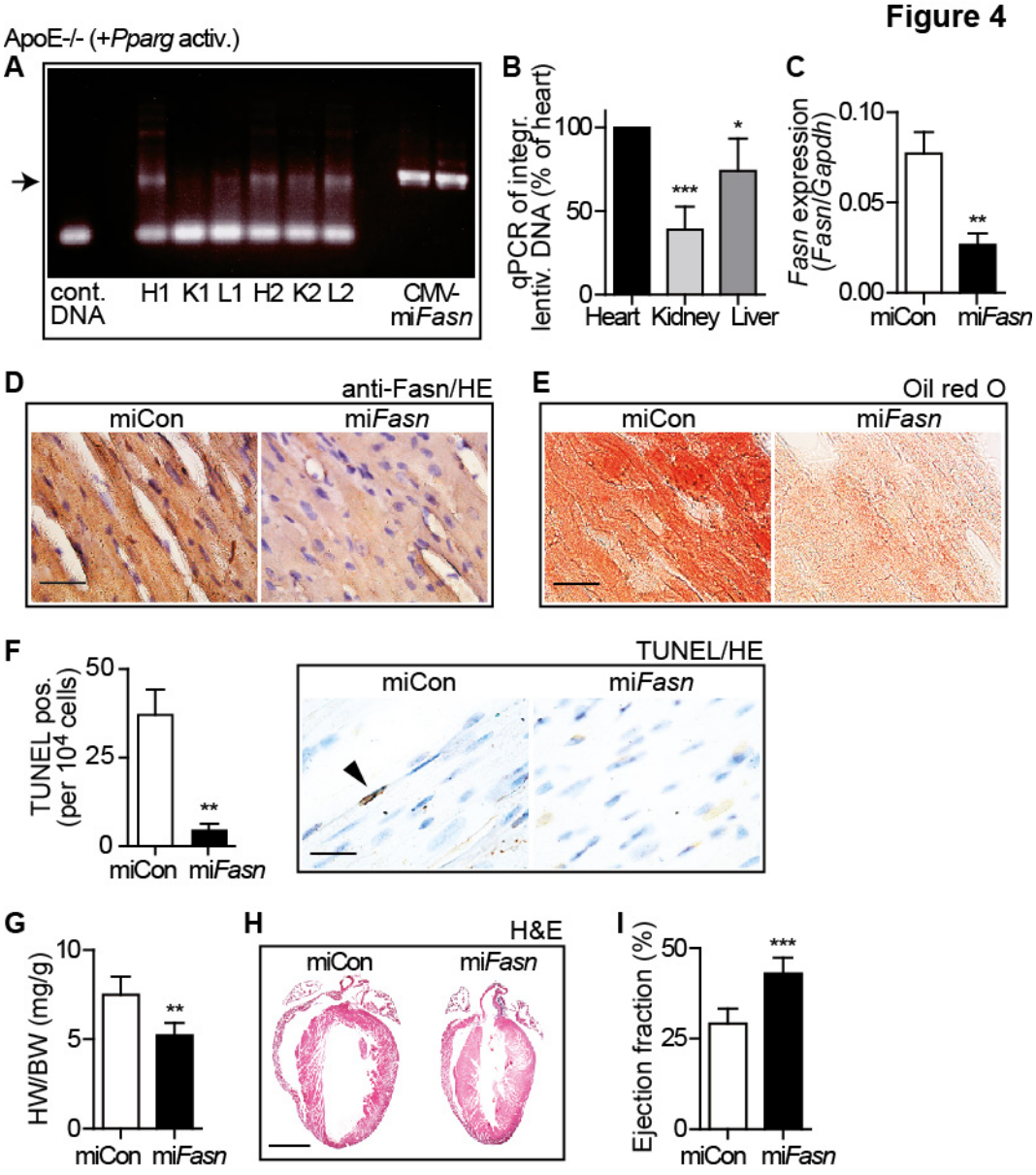

**Figure 5**

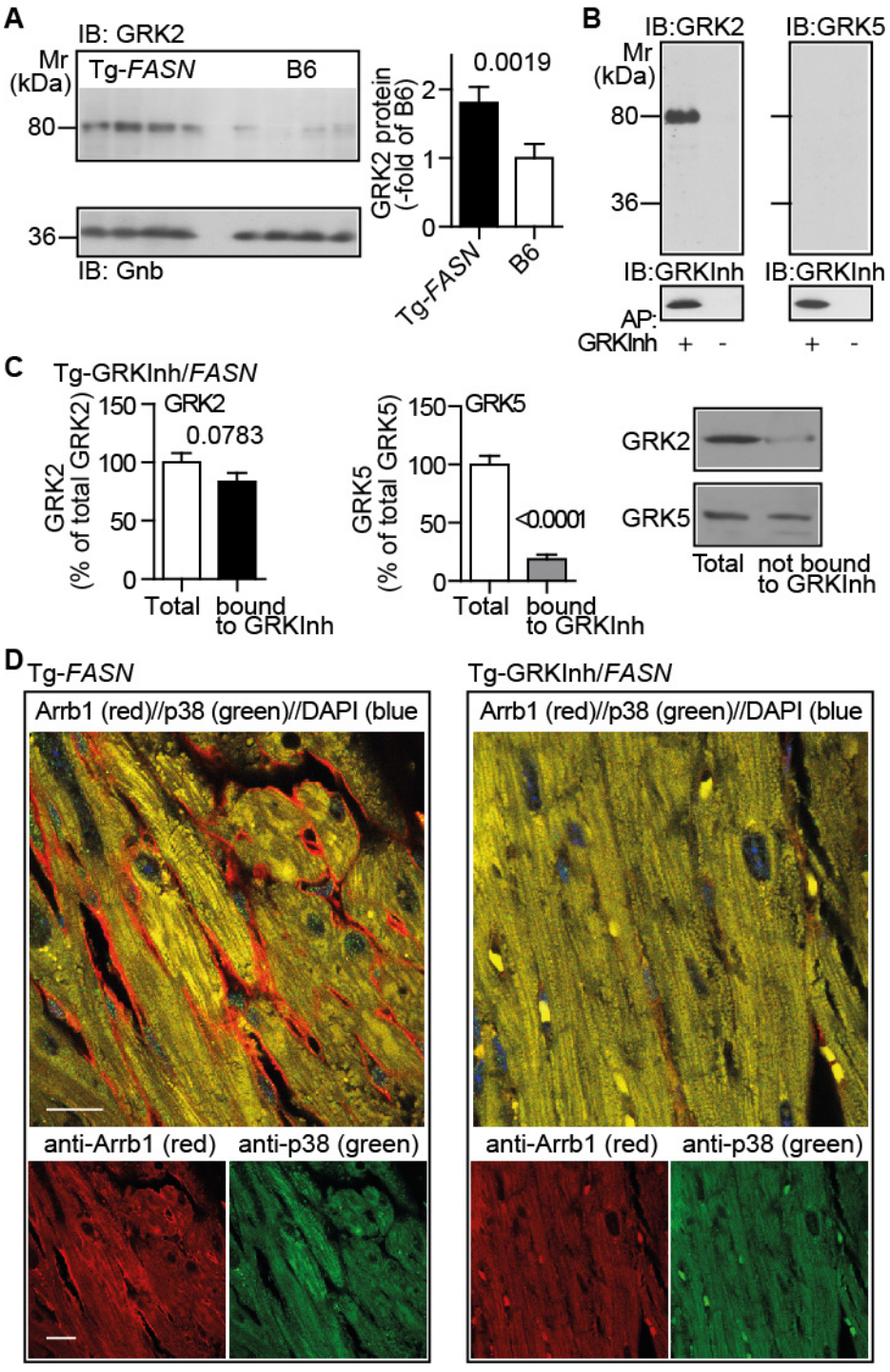

**Figure 6**

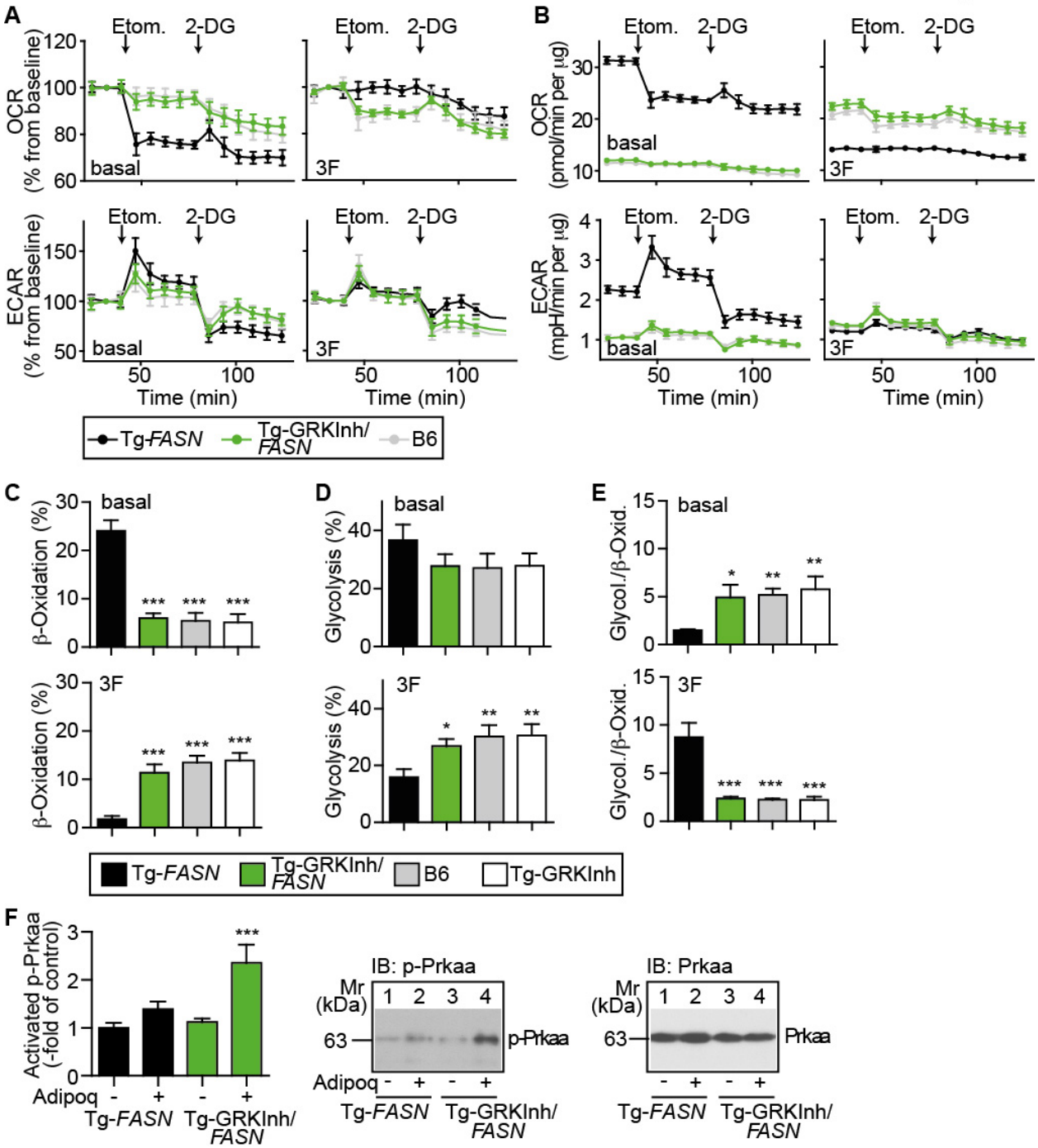

**Figure 7**

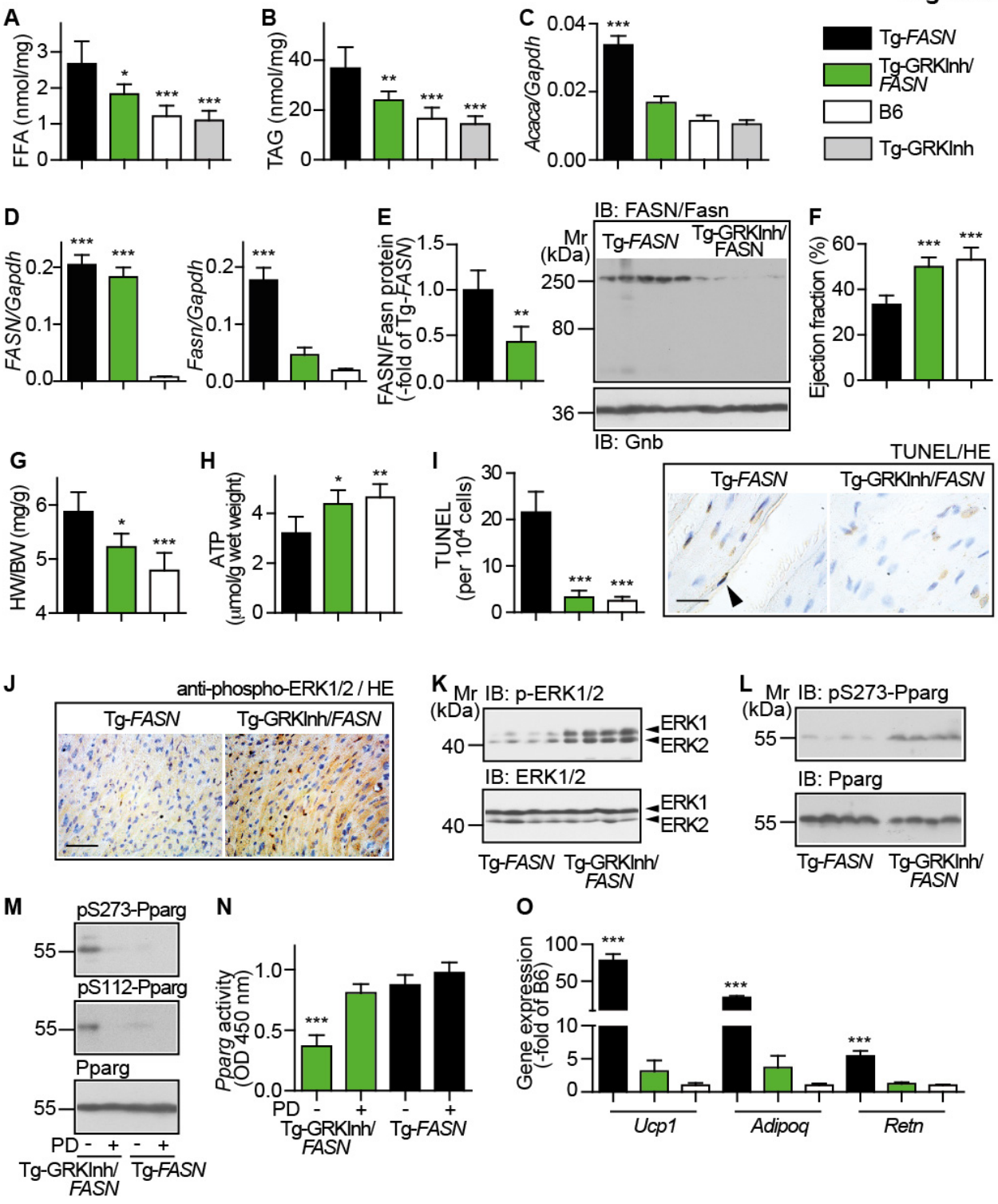

**Figure 8**

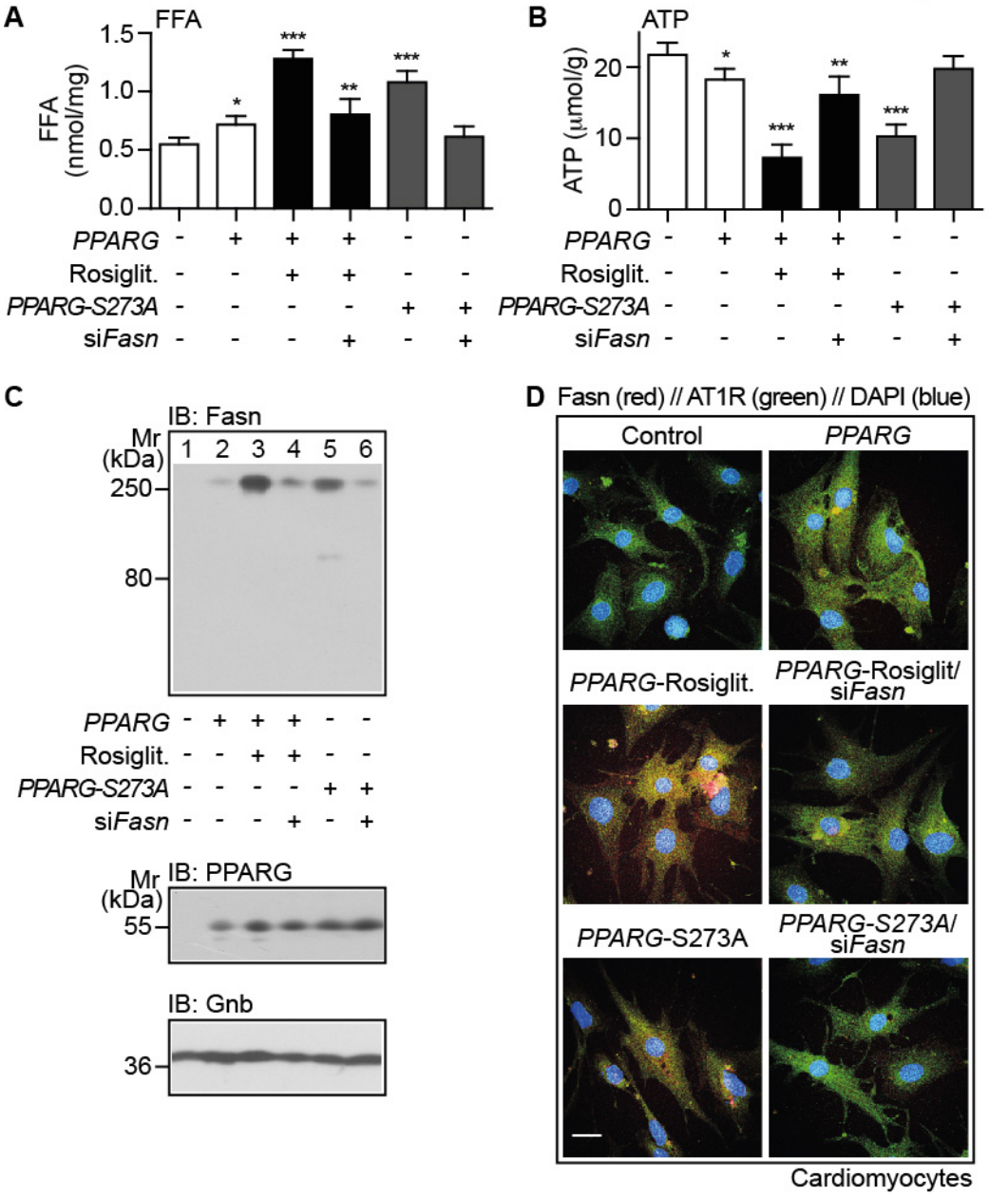

**Figure 9**

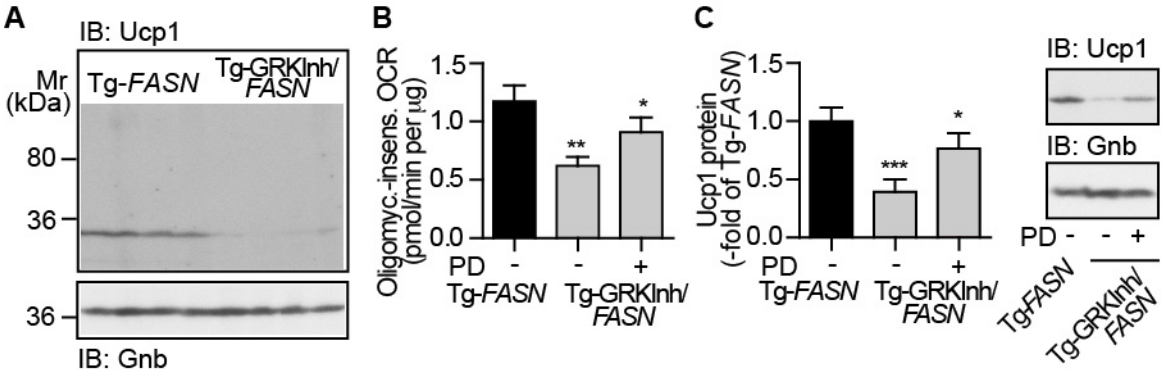

**Figure 10**

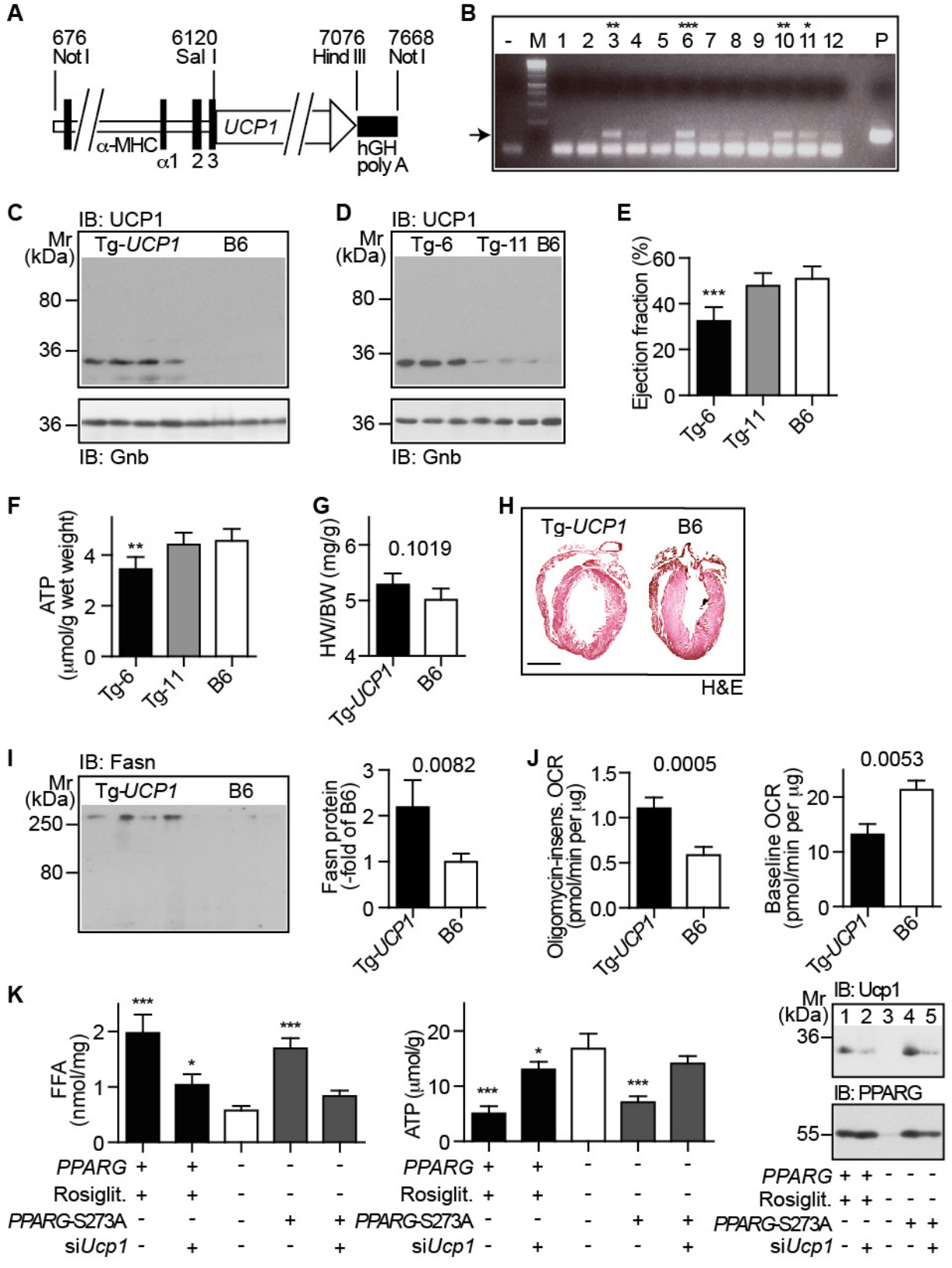

**Figure 11**

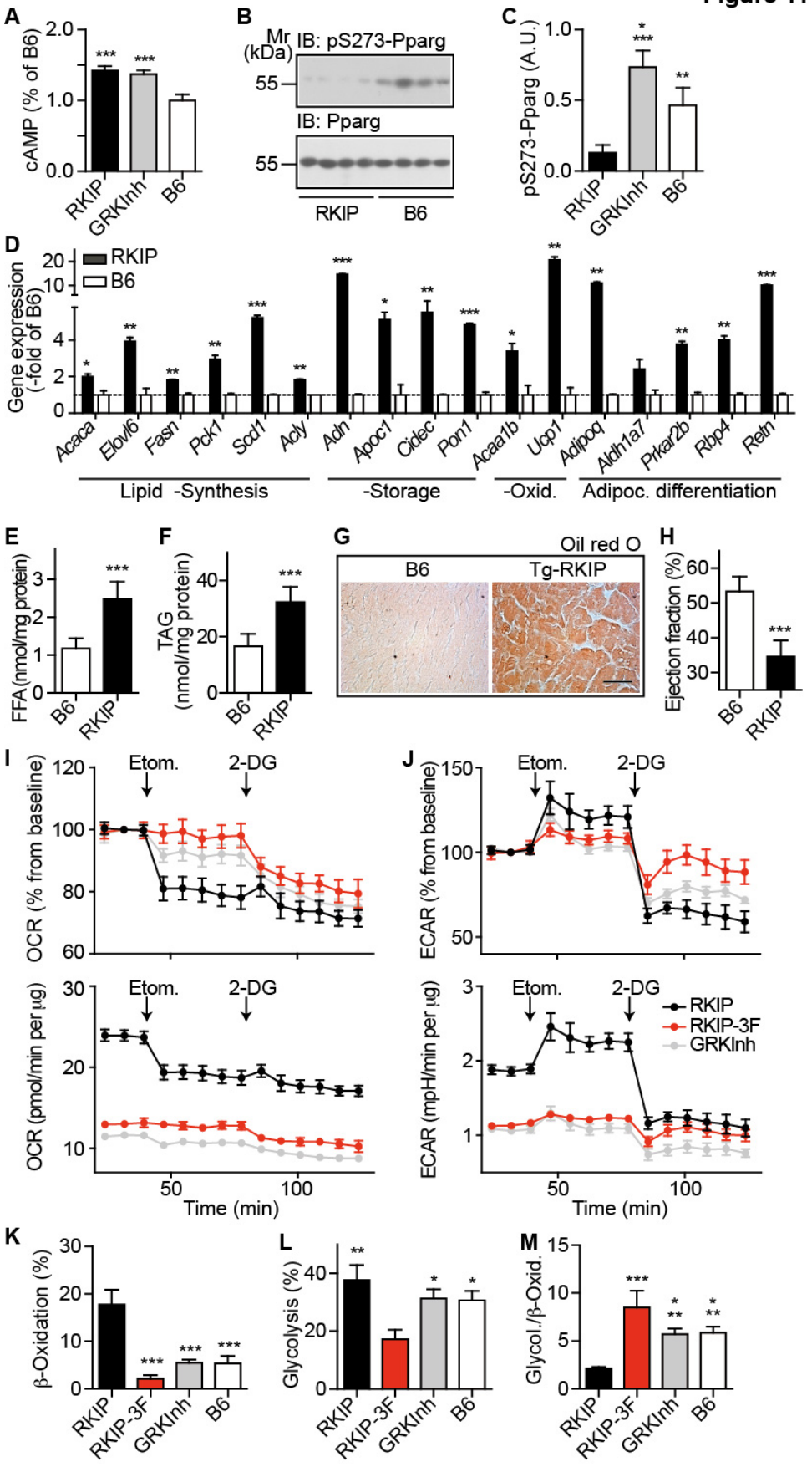

**Figure 12**

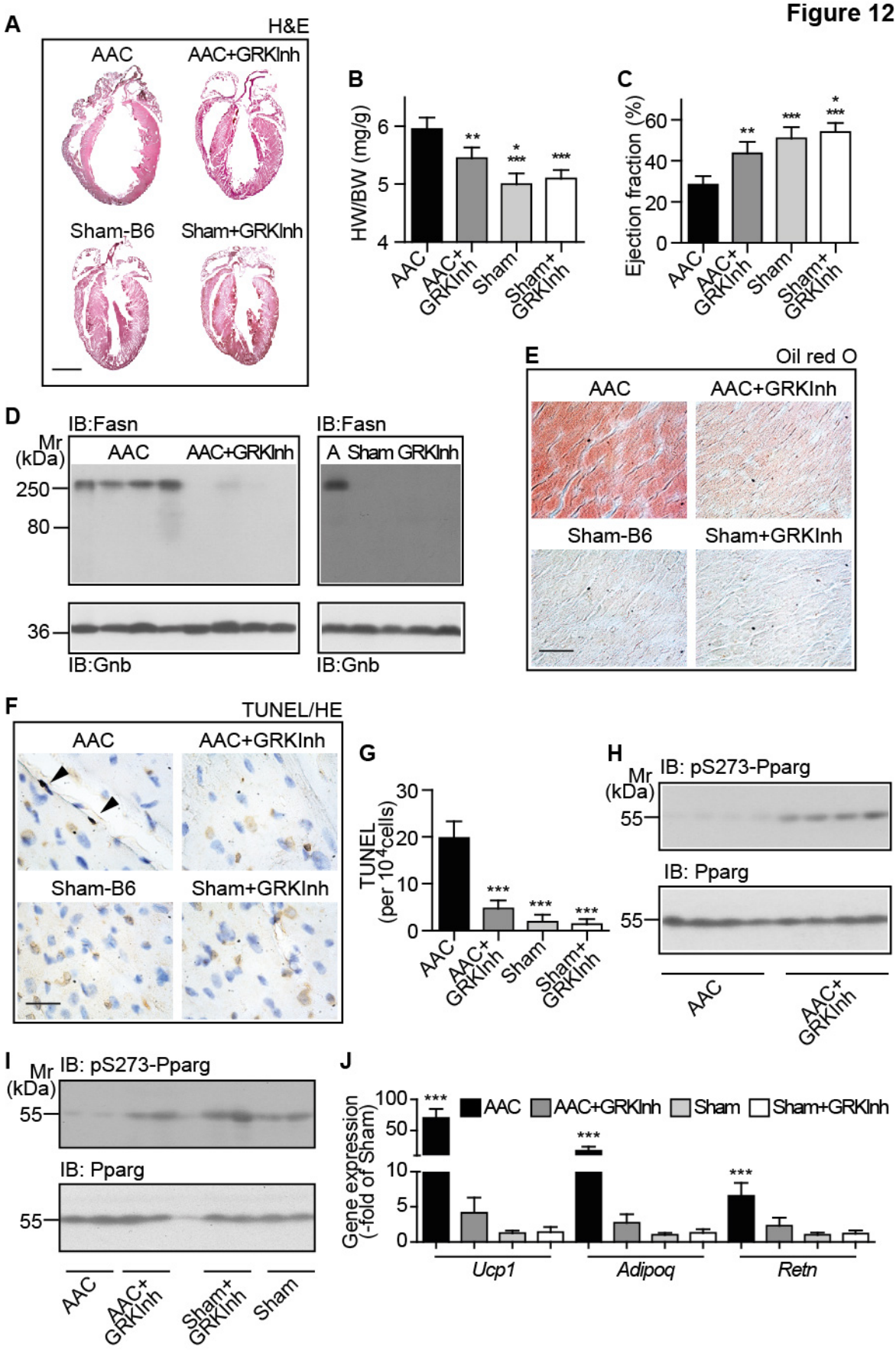

**Figure 13**

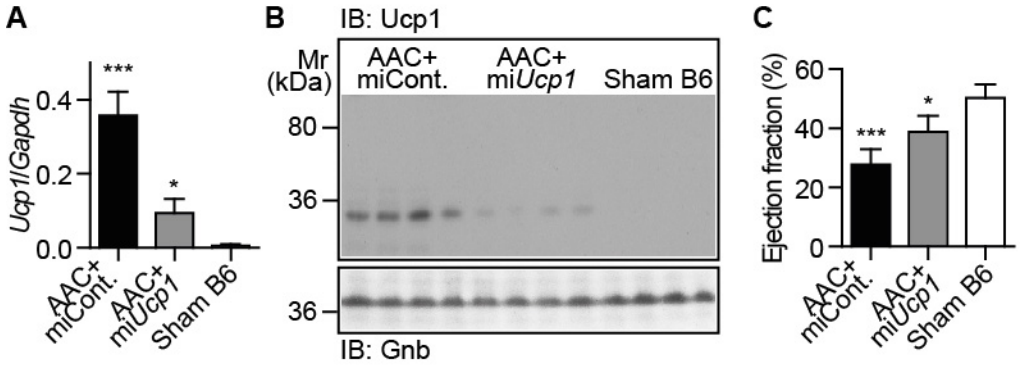

**Figure 14**

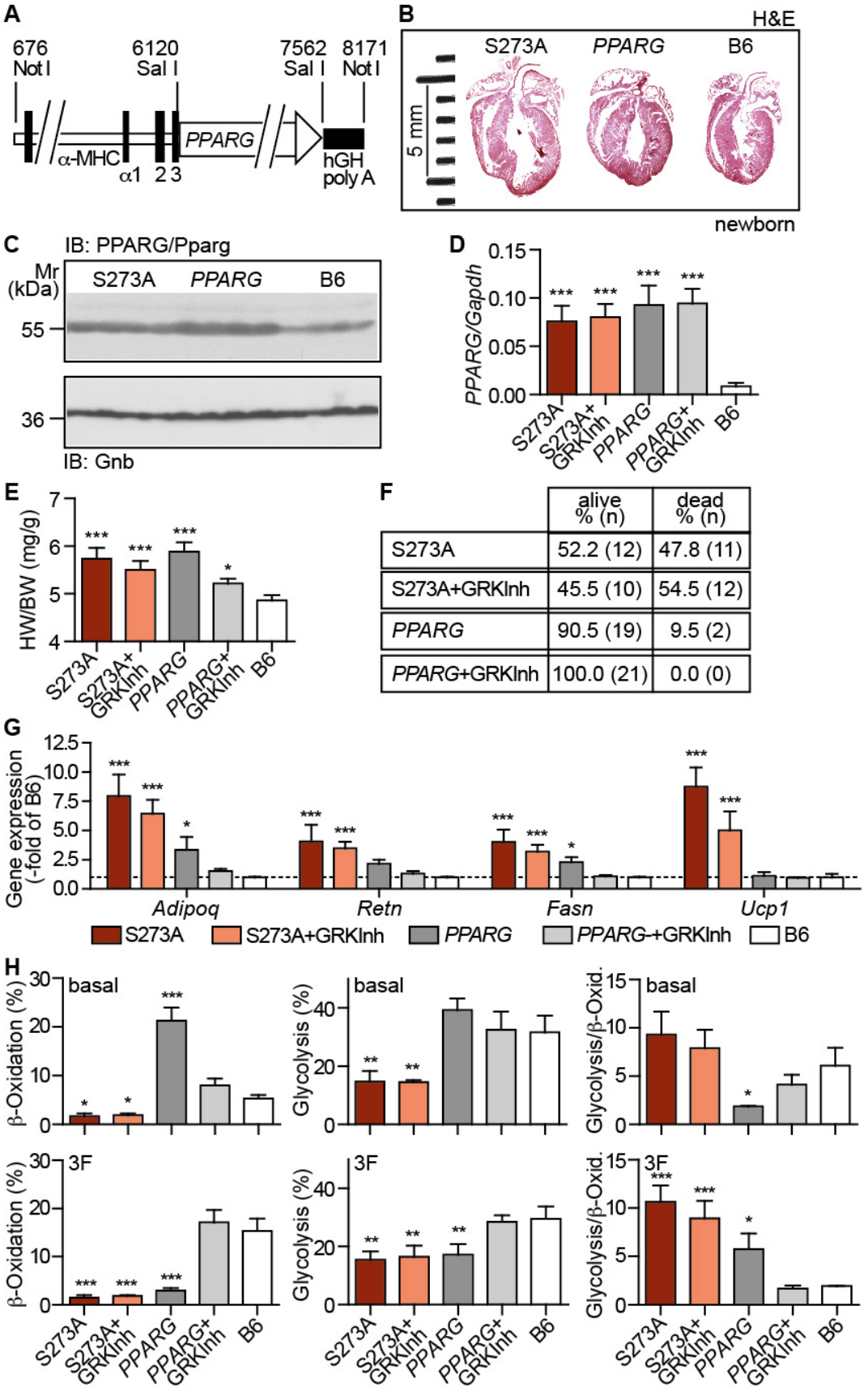

**Figure 15**

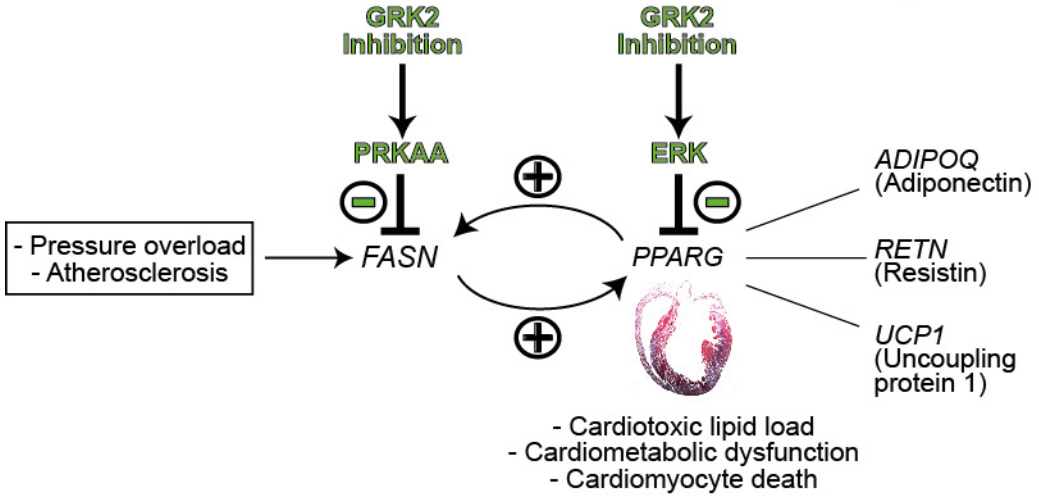

# Inhibition of G-protein-coupled receptor kinase 2 prevents the dysfunctional cardiac substrate metabolism in fatty acid synthase-transgenic mice

Joshua Abd Alla, Muriel Graemer, Xuebin Fu and Ursula Quitterer

*J. Biol. Chem. published online December 15, 2015*